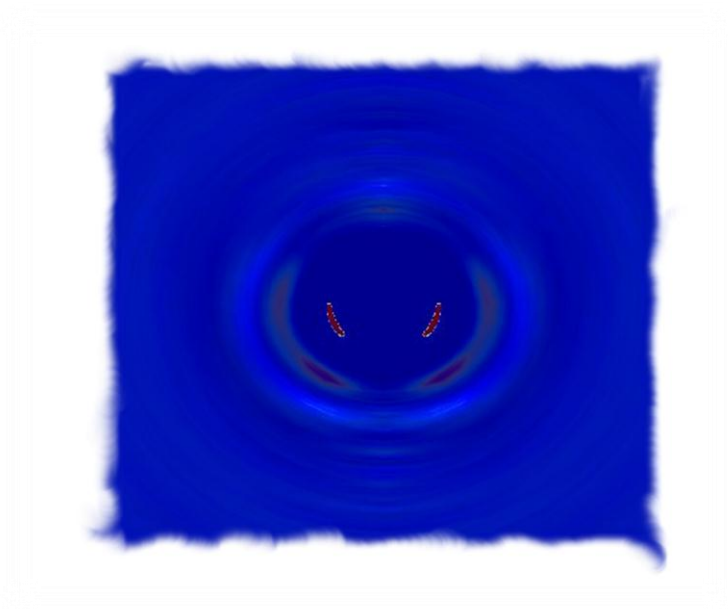


Asymmetric and Symmetric Hydration of Hydrated Anions in Aqueous Solution

Lars Eklund

*Faculty of Natural Resources and Agricultural Sciences
Department of Chemistry
Uppsala*



Licentiate Thesis
Swedish University of Agricultural Sciences
Uppsala 2011

ISBN 978-91-576-9040-1
© 2011 Lars Eklund, Uppsala
Print: SLU Service/Repro, Uppsala 2011

Cover: ARD sulfur to hydrogen sulfur to oxygen distances of hydrated sulfite ion in aqueous solution(Lars Eklund 2011)

Asymmetric and Symmetric Hydration of Hydrated Anions in Aqueous Solution

Abstract

The interaction between solvent and solute is a very important chemical property that has large impact on the chemical reactions taking place. In Paper I and II the structure of hydrated sulfite, selenite and selenate in aqueous solutions are determined and compared. The sulfite is also compared with earlier work and new work has been done to show the difference in symmetric and asymmetric hydration. The first hydration shell of sulfite and selenite has been shown to be asymmetric with large influences on the properties of these ionic aqueous solutions, it is therefore vital that these structures are known. Furthermore, the polyatomic anions studied have been shown to be structure makers, and this greatly affects the thermodynamic properties of the solutions. One can conclude that the series of the solutions, from weakest to strongest structure maker, is selenite < selenate < sulfite < sulfate. This indicates a trend in the hydration behavior of oxoanions where higher oxidation and symmetry leads to stronger structure making behavior in addition to the expected effect generated by increased charge density. In conclusion, the effects of asymmetric hydration can be seen in the ions studied with great effect to the physico-chemical properties of the hydrated ions and the reactions that they are involved in.

Keywords: Hydration, selenite, selenate, sulfite, sulfate, anion, ARD, RDF, LAXS, DDIR, asymmetric hydration, symmetric hydration, QMCF

Author's address: Eklund Lars, SLU, Department of Chemistry,
P.O. Box 7082 Uppsala, Sweden
E-mail: Lars.Eklund@slu.se

Dedication

To my loving wife for giving me strength and support throughout the process.

“Before beginning a Hunt, it is wise to ask someone what you are looking for before you begin looking for it.”

Inspired by Alan Alexander Milne “Winne the Pooh, Pooh’s little instruction book”

Contents

<i>List of Publications</i>	6
<i>Abbreviations</i>	8
1 <i>Introduction</i>	9
1.1 Chemical nature of water	9
1.2 Coordination chemistry , what is behind the coordination number of hydrated anions	10
1.3 Hydrogen bonding	11
1.4 LAXS methodology	12
1.5 Computational methodology, the QMCF	14
2 <i>Results</i>	17
2.1 Sulfoxo anions	17
2.1.1 Hydrated sulfite ion	17
2.1.2 Comparison of hydrated sulfite and sulfate ions	18
2.2 Hydrated selenite and selenate ions	19
2.3 Comparison of oxo sulfur and oxo selenium anions	20
3 <i>Conclusion</i>	22
<i>References</i>	23
<i>Acknowledgements</i>	24

List of Publications

This thesis is based on the work contained in the following papers, referred to by Roman numerals in the text:

- I Eklund L., Hofer T., Pribil A., Rode B.M., Persson I. (2011). On the Structure and Dynamics of the Asymmetrically Hydrated Sulfite Ion in Aqueous Solution – An ab initio QMCF MD Simulation and Large Angle X-ray Scattering Study. *Manuscript*.
- II Eklund L, Persson I.(2011). Comparative structure studies of sodium selenate and sodium selenite using large angle X-ray scattering and double differentiated FTIR. *Manuscript*.

The contribution of Lars Eklund to the papers included in this thesis was as follows:

- I All computational workup except the sulfate ARD in collaboration with Thomas Hofer and Andreas Priblil and major contributions to the text
- II All IR experimental work. Analysis and compilation of experimental data of selenite and was a contributor to the text.

Abbreviations

RDF	Radial Distribution Function
ARD	Angular Radial Distribution function
ADF	Angular Distribution Function
MRT	Mean Residence Time
QMCF	Quantum Mechanical Charged Field
LAXS	Large Angle X-ray Scattering
FT-IR	Fourier Transformed Infra-Red spectroscopy
DDIR	Double Differential fourier transformed Infra-Red spectroscopy
QM/MD	Quantum Mechanical /Molecular Dynamics
CN	Coordination Number
BJH-CF2	Bopp, Jancsó and Heinzinger modification to central force model, force potentials for water.
FWHH	Full Width Half Height
FWHM	Full Width Half Maximum, equivalent of FWHH

1 Introduction

1.1 Chemical nature of water

Water is one of the most important chemicals and the most common solvent on the planet. It has unrivaled importance for the chemistry of life as it is the solvent in all biological systems and the only naturally occurring solvent on earth. To understand the chemistry of solutions the chemical properties of the solvent have to be considered and understood. Therefore, to understand many of the commonly occurring chemical reactions we must understand water. Water is a dipolar molecule of oxygen and hydrogen, where the dipolar moment comes from the difference in electron density along the axis of symmetry. The large free electron pairs on the oxygen cause a bonding angle of 105.4° which gives the water molecules many of its intriguing qualities as a solvent. The all hydrogen and oxygen of water partake in hydrogen bonds, giving water both accessible acceptors and donors generating strong intermolecular forces through hydrogen bonding. This gives a high degree of order in the liquid water. The strong cohesiveness of water is reflected in its properties such as surface tension and boiling point which is high comparing to liquids such as benzene or diethylether where the primary intermolecular force is van der Waals interactions or weak dipol-dipol interactions. The structure of liquid water is dominated by the hydrogen bonds with a intermolecular distance of 2.89 \AA as determined by X-ray spectroscopy. The intermolecular distance is affected locally when a solute is introduced to water, either becoming shorter or longer. This effect divides the solutes into structure maker and structure breaker (Marcus, 2009) and is observable for dilute solutions the classification is considered problematic for higher concentrations (Bakker, 2008). In short, the fascinating properties of water as a solvent is governed by hydrogen bonding and its ability to hydrogen bond to solutes is paramount

to understanding reactions that occur in water and therefore vital in understanding any biological system. The fact that water is an environmentally safe solvent means that many of the reaction systems studied in the future will depend on the knowledge of water as a solvent. This thesis is aimed at understanding the interactions between water and polyatomic anions.

1.2 Coordination chemistry, what is behind the coordination number of hydrated anions

A coordination entity is defined as a central atom to which a surrounding array of groups of atoms is attached (Nič et al., 2009a). The central atom is usually a metal in the case of cations. In anions there is a large diversity of negatively charged single atom ions and polyatomic anions. This work will deal with some of the issues related to polyatomic anions. In the case of polyatomic anions the central atom is the entire covalently bound anionic species, and the surrounding ligands interact with it by hydrogen bonding or other electrostatic interactions.

The coordination number (CN) is the number of ligands bound in a coordination entity, for hydrated anions this means the number of water molecules hydrogen bound to the central ion. The CN is usually defined for a given coordination shell, where a coordination shell can be defined as the ligands binding to the central entity in the same way. The coordination shell in hydrated coordination species are called hydration shells, and the first hydration shell is the water molecules directly binding through electrostatic interactions to the solute. For the second hydration shell the definition used here is waters that are bridged by atoms in the first hydration shell. Any further shells are of course defined analogously until we find water molecules whose binding behavior is no different than that of the bulk. The ions discussed in paper I and II have a small interaction difference in the first shell compared to bulk water. This means that defining shells extending beyond the first is not relevant since there is no discernable difference from bulk behavior. There has been very little published on the coordination of polyatomic anions, especially on oxoanions, but the coordination number is for complex anions high. For the oxoanions a 12-coordination seems to be quite common, this 12-coordination is more transient than in the commonly studied metal ion coordination and calling it coordination number according to the Inorganic nomenclature (Nič et al., 2009b) may be

to over-emphasize the amount of order. Although these coordination entities contains several atoms with mostly uniform binding, in some cases different binding between central ion and bound ligand occurs and therefore the weaker term occupancy would probably be better. This would signify the slightly weaker bonding restriction than the formal CN would allow for. The use of CN as an acceptable term comes from the similarities in techniques employed to study the occupancy in asymmetrically hydrated species and symmetrically hydrated species. The mechanisms of coordination is a phenomenon of electrostatic interactions, in metal cations it is usually caused by overlap of metal d orbitals with sigma orbitals of the ligand, while in the case of anions it is mostly lone pair electrons in pi orbitals interacting with sigma orbitals of the ligand. This gives longer distances corresponding to the potential minima for the anions than for the cations. The anionic coordination also has much higher exchange rates than corresponding metal complex and using designations of the coordination symmetry as is done with metal complexes might lead the reader to envision a stable structure where there is none. Whereas using the accepted term CN is recommended to describe the existence of direct interactions. The coordination is a phenomenon of electrostatic interactions which in aqueous solutions are dominated by hydrogen bonds and hydrogen bond-like interactions.

1.3 Hydrogen bonding

Many definitions of a hydrogen bond exist; their lowest common denominator is that hydrogen is bound to two or more atoms. Huheey et. al. states that some may view it as nothing more than an extreme dipole-dipole bond (Huheey, 1993), but most would agree that it is convenient to separate it from other bonds as its strength sets it apart and hydrogen bonds play a major role in defining the properties of the chemical species that participate.

Atkins defines the most elementary description as a coulombic interaction between the partially exposed positive charge of a proton bound to an electron withdrawing atom and the negative charge of a lone-pair of the second atom (Atkins, 2000). Using an energetic definition the hydrogen bond can be described as having a potential well minimum which is at a distance which means that the hydrogen overlaps the bonding atoms in such a way that the electron cloud is deformed. The hydrogen forms a bridge which allows for the formation of two bonds to the hydrogen by sharing the electron over the sigma bond. It is important to note that the border where an bond becomes a hydrogen bond is not clearly defined as it is dependent

on the binding species and that there exists cases where the deformation of the electron cloud exists and a charge interaction fulfill the definitions but it is still not convenient to consider it a hydrogen bond. Such is the case of sulfur or selenite lone-pair interaction. It is convenient not to consider these as hydrogen bonds due to their difference in kinetic behavior, thereby distinguishing them from the hydrogen bond from water to oxygen on the oxoanion and hydrogen bonds formed between water molecules of the solution.

1.4 LAXS methodology

The Large Angle X-ray Scattering builds on the principle of electrons scattering X-ray radiation. This is detailed in earlier work (Persson, 1984) but a short summation is presented here. When an X-ray beam is directed at a sample, the incoming radiation may scatter when hitting electrons in the sample. Such scattering events can be detected by measuring the intensity of the beam after the sample at several angles. This is done using a $\Theta - \Theta$ goniometer. When the intensities for each angle has been collected the scattered intensities has to be transformed to the physical structure of the solution. This is done by using the form factors which is the amount a given electron around an atom scatters the incoming radiation, these are labeled f_e . It is convenient to introduce the parameter s where $s = 4\pi \sin\Theta/\lambda$ which means the scattering for one electron assuming spherical charge distribution is

$$f_e = \int_0^{\infty} 4\pi r^2 \rho(r) \frac{\sin sr}{sr} dr$$

The amplitude for scattering from an atom with several electrons is simply the summation of f_e for each electron. The treatment of atomic scattering factors is dependent on two assumptions

- I) The X-ray wavelength is much smaller than any absorption edge wavelengths in the atom.
- II) The electrons are distributed according to spherical symmetry.

When assumption I) fails a dispersion correction is needed so that the expression becomes $f = f_0 + \Delta f' + i\Delta f''$, where f is the corrected scattering factor and f_0 is the atomic scattering factors. The anomalous scattering factors f' and f'' correct for the anomalous dispersion. The imaginary part f'' represents a small shift in the phase of the scattered radiation and its angular dependency is much lower than the angular dependence of f_0 .

Once the electron scattering is determined the Compton scattering can be determined as $i_c = 1 - f_c^2$. Because the Compton scattering is coherent for different electrons the intensity is the sum of the electron Compton scattering. Compton scattering is dependent on the Breit-Dirac factor R which is dependent on the type of detector used. Given the random orientation in a gas, liquid, amorphous or powdered crystalline sample the intensities in the sample is

$$I_{cu} = \sum_m \sum_n f_m f_n \frac{\sin sr_{mn}}{sr_{mn}}$$

which is the Debye scattering equation taking into account the Compton scattering. A molecule will give the intensity as $I/N = I_{cu} + R \sum_i i(c)$ with N as the number of molecules in the sample. If we now are to extend the Debye including Compton scattering to work in solutions with more than one kind of molecules we need to construct a set of pair functions correlating to the different distances between the species I and J

$$W_{IJ} = \int_0^{s_{\max}} \frac{f_I f_J}{g^2(s)} e^{-\alpha^2 s^2} \sin sr_{IJ} ds$$

Where $g(s)$ is a sharpening function and α is a convergence coefficient. Through Fourier transformation a radial distribution function can be constructed

$$D(r) = \frac{2r}{\pi} \sum \sum \frac{N_{IJ}}{r_{IJ}} W_{IJ}(r)$$

When plotting $D(r)$ vs r the interatomic distances in the sample are given by the peak positions. The temperature factor (b) for the distance assuming harmonic motion and gaussian distribution can be expressed as $b = l^2/2$ where l is root mean square of the variation, σ , is related to the full width at half height (FWHH), as $FWHH = 2\sqrt{2 \ln 2} \sigma$

The term FWHH is commonly used in spectroscopy and interchangeable with the term full width at half maximum FWHM.

Using the above equation means that one can assess the interatomic distances from the measurement of intensities of scattered X-ray radiation and angle.

1.5 Computational methodology, the QMCF

The Quantum Mechanical Charged Field QM/MD molecular simulation technique (Rode et al., 2006, Rode & Hofer, 2006) combines a quantum region (spheres in *Figure 1*) with a bulk region calculated using classical Molecular Mechanics (box in *Figure 1*). The Quantum region has a core region (inner sphere in *Figure 1*) where all except long range columbic interactions can be calculated with a pure quantum mechanical approach and boarder layer (outer sphere in *Figure 1*) in which calculations are done quantum mechanically and by adding a smoothing term towards the MM potentials, the smoothing region is a thin region at the edge of the solvation layer. By using a water model that allows for explicit hydrogen moments we address the problem of overestimation of exchange events.

The use of electrostatic embedding procedures, where the point-charges of the MM molecules are included in the QM calculations, is used in order to polarize the molecular orbitals to avoid surface artifacts resulting from calculation in artificial vacuum. Therefore the force on each paticle J in the core F_J^{core} is

$$F_J^{\text{core}} = F_J^{\text{QM}} + \sum_{I=1}^M \frac{q_j^{\text{QM}} \cdot q_I^{\text{MM}}}{r_{JI}^2} \cdot \left[1 + 2 \cdot \frac{\epsilon + 1}{2\epsilon - 1} \cdot \left(\frac{r_{JI}}{r_c} \right)^3 \right]$$

Where the first component F_J^{QM} is the quantum mechanical treatment including embedding of partial charges. The second part accounts for columbic interactions between particle J and all MM atoms as described by the set M . A population analysis of the molecules in the QM region gives their contribution for the MM molecules as partial charges using the reaction field method (last part) to compensate for the error introduced by the use of a cutoff radius. The reaction field accounts for the influence of surrounding medium beyond the cutoff distance r_c as a function of the dielectric constant ϵ . In the layer region an additional force term for the non-columbic interactions has to be added resulting from non-columbic

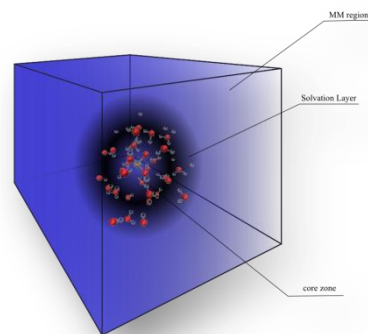


Figure 1. A schematic picture of the simulation box containing the QM core region, inner sphere, the QM solvation layer, outer sphere, and the Molecular Mechanical region showing the boundaries of the box.

interactions between the layer atom and the MM atoms. The force for the MM atoms F_J^{MM} is calculated by taking into account the columbic forces from the QM region, the non-columbic interactions from the layer region and a reaction field compensating for the cut off distance as a function of the dielectric constant. This results in the following force equation

$$F_J^{MM} = \sum_{\substack{I=1 \\ I \neq J}}^M F_{IJ}^{MM} + \sum_{I=1}^{N_1+N_2} \left\{ \frac{q_I^{QM} \cdot q_J^{MM}}{r_{IJ}^2} \cdot \left[1 + 2 \frac{\epsilon + 1}{2\epsilon - 1} \cdot \left(\frac{r_{IJ}}{r_c} \right)^3 \right] \right\} + \sum_{I=1}^{N_2} F_{IJ}^{nC}$$

The first part of the above equation is the classical MM part for M-1 pairwise interactions with particle J. It contains columbic non columbic and intramolecular force field contributions. The second part is the charged field interaction term for all core atoms N_1 and all layer atoms N_2 . These force contributions are equivalent to the columbic force contributions in the QM region thereby conserving force consistency and momentum. Finally, the last factor is the non-columbic interactions with the layer region again ensuring force consistency and momentum. As with all QM/MM applications a smoothing function has to be applied for any particle J transitioning from the quantum region to the mechanics region. This smoothing function F_J^{smooth} ensures continuous transition of the forces upon migration. If one does not use a flexible solvent model such as BJH-CF2, then the inability to account for intramolecluar motion will generate artifacts in the transitioning molecular forces. For all molecules in the smoothing region the force evaluation is duplicated, once as a QM layer atom and once using MM with the resulting force as

$$F_J^{smooth} = S(r) \cdot (F_J^{layer} - F_J^{MM}) + F_J^{MM}$$

Where $S(r)$ is a continuous function defined as

$$S(r) = 1, r \leq r_1$$

$$S(r) = \frac{(r_0^2 - r^2)^2 (r_0^2 + 2r^2 - 3r_1^2)}{(r_0^2 - r_1^2)^3}, r_1 < r \leq r_0$$

$$S(r) = 0, r > r_0$$

In the smoothing factor $S(r)$ r is the distance between a given solvent molecule's centre of mass and the centre of the QM region. r_0 is the radius of the layer region and r_1 is the inner border of the smoothing region. This simple function generates a slight violation of the momentum conservation but the effect generates a small enough deviation not to be noticeable over the normal course of a simulation run. In addition this effect is dependent

on the thickness of the smoothing region, if a too thick region is chosen a significant violation of the momentum conservation occurs. Considering the computational effort in using a more complex smoothing evaluation scheme these errors are most effectively handled by giving a thin enough smoothing region and checking the momentum during the simulation. The thickness used in the sulfite simulations was 0.2 Å. Using the above method one can generate simulated data which can be analysed using i.e. Pair potentials, trajectory data and much more. The trajectories can be analysed using different sets of RDFs, using pairwise population analysis, Using an angular division of the coordination sphere information about the arrangement of the hydration if it is symmetrical or asymmetrical.

2 Results and Discussion

2.1 Sulfoxo anions

2.1.1 Hydrated sulfite ion

The hydration of the sulfite ion in aqueous solution, has been shown to be asymmetrical, this can be seen by studying the distances in the radial rdf (paper I) where two different sulfur to oxygen distances are observed, one shorter at 3.68 and 3.73 Å, and one longer at 4.16 and 4.11 Å, as determined by LAXS and QMCF respectively. The shorter distance corresponds to the water oxygen bound through hydrogen bonding to the oxygens of the sulfite ion. The water oxygens clustered outside of the sulfur lone-pair electrons interact with the ion through weak electrostatic interactions with the water dipole. The waters are oriented with hydrogen towards the ion for all waters in the hydration shell interacting with the ion, this is

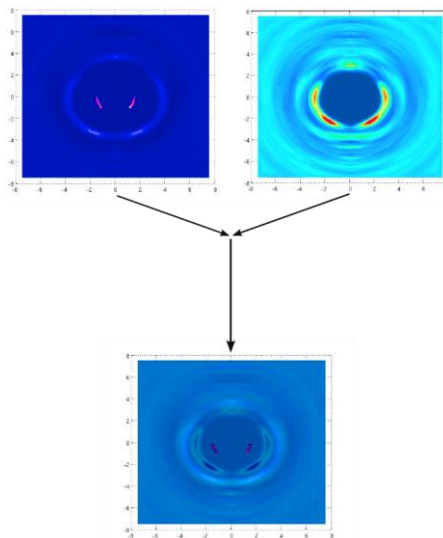


Figure 2. The combination of sulfite ARD of oxygen sulfur distances of hydrated sulfite (left), and sulfur hydrogen distances (right). The combined plots (bottom) show that the hydrogen of water in the first hydration sphere are localized and oriented towards the ion and closer to the ion than the corresponding water oxygen.

clear from the ARD of the simulation (*Figure 2* showing the combination of

sulfur oxygen ARD(left panel) and sulfur Hydrogen ARD(right panel)). The average coordination number from simulation coincides well with the coordination determined by the LAXS experiment (CN 12). There is a slight over estimation of coordination with simulation data averaging at CN 12.3. This over estimation originates from two sources, the use of Haartree Fock level of theory and the use of symmetric analysis of the hydration.

2.1.2 Comparison of hydrated sulfite and sulfate ions

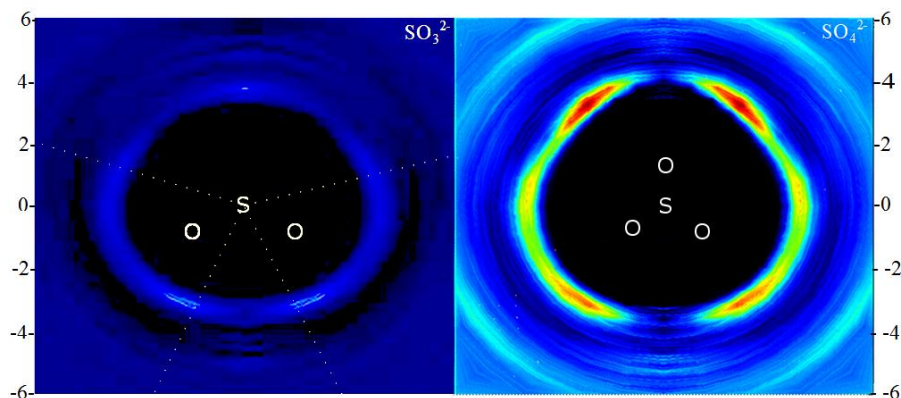


Figure 3. The Angular Radial Distribution of water oxygens around the sulfite and sulfate ion respectively. The images have a common base intensity where the black region denotes no oxygen occupancy during the entire simulation. The white dashed lines in the sulfite delimit regions where no direct interchange has happened between first hydration shell and bulk water.

When comparing the sulfite and sulfate ions, Paper I, one can see differences in that there are two distinct distances for sulfite to water in the first hydration shell but only one in hydrated sulfate in aqueous solution. This implies that there are different properties of the waters binding to the sulfur compared to the oxygens of hydrated sulfite. This becomes even more pronounced when studying the dynamics of the system using angular radial distribution function from the QMCF simulations. As we compare the hydrated sulfite ion and sulfate ion in the ARD (*Figure 3*), the left side show the angular radial distribution function for the water oxygens in hydrated sulfite ion and the right show the analogue of sulfate, in the image the approximate position of the central ion has been indicated. In *Figure 3* there are areas where no water oxygen has occupied that particular (angle, distance) coordinate (black) it is therefore logical to conclude that no direct exchange can happen across these areas as a molecule traveling from one point in space to another must occupy all intersecting points in space at

some time during its trajectory. In the sulfate these areas are as expected strictly located to the space occupied by the ion meaning that the hydration exchange is symmetrical. In the hydrated sulfite ion locating the same areas there are of course the space occupied by the ion itself and more unexpected areas located in between the first hydration shell and the bulk. This generates an asymmetric exchange across the hydration sphere so that when studying the system using symmetrical tools such as the MRT we get an under estimation of the actual exchange times in the sectors where actual exchange occur between waters of the first hydration shell and the bulk water. Unfortunately the MRT values only represent the actual dynamics of the system for a symmetric system as it is the number of exchange over a sphere over a given time, this means that the actual exchange rate is faster for the sulfite ion than they appear using MRT analysis as can be interpreted using the information from the ARD, *Figure 3*.

2.2 Hydrated selenite and selenate ions

The selenate and selenite ions were studied using LAXS and DDIR, Paper II. It was shown that the solvated selenite ion contained two distinct hydration distances $\text{Se}-\text{O}_w$ 3.68 Å and 4.36 Å in comparison to the selenate

ion which only has one at 3.94 Å. This shows an asymmetric hydration structure for selenite. It can further be seen that the electrostatic interactions of

the partially reduced selenite has a longer mean distance and somewhat lower effect on the surrounding water. Overlay of experimental RDF for selenite and selenate ion, *Figure 4*, show the difference in short distances with the selenate having slightly longer and broader profiles for the $\text{O}(\text{Se})\dots\text{O}(\text{w})$ and slightly longer internal Se-O distances. At longer distances the effect is negligible. This is consistent with both selenite and selenate ions having negligible impact on the water structure beyond the first shell. The treatment of affected number detailed elsewhere (Kristiansson &

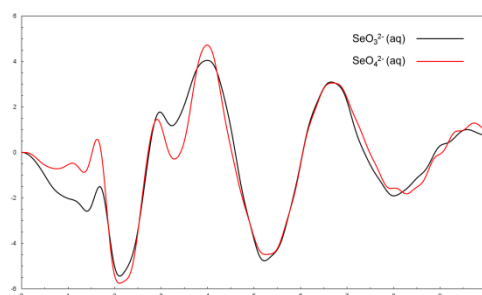


Figure 4. Overlay of experimental RDF for selenite and selenate ion, show the difference in short distances with the selenate having slightly longer and broader profiles for the $\text{O}(\text{Se})\dots\text{O}(\text{w})$ and slightly longer internal Se-O distances.

Lindgren, 1991), show the complexities of interpreting physical parameters from affected number and indeed in the systems studied the correlation between affected number and CN is low. The separated anion and cation bands show that selenite and selenate ions can be consider as weak structure makers based on peak position and thereby hydrogen bond strength. This means that their local solvation structure is stronger than that of pure water. In *Table 1* the Se-O distances for some ionic species of selenium has been listed comparing the solvated species and the crystal phase equivalent. There is a 0.04 and 0.07 Å elongation in the aqueous selenite and selenate-ions respectively. It is also clear that there is a elongation occurring with decrease in oxidation of the Selenium as the charge density decreases also the effect of binding ligands or atoms can be seen in the elongation of distances as the affected selenium oxygen distances are elongated.

Table 1. Mean Se-O distances in Ångström(Å) work presentet in Paper II, (b) refers to literature mean values Table S1, Paper II. The * refer to mean values of two mean values for distances depending on hydrogen configuration.

Ion	Mean Se-O distance(Å)
SeO ₃ ²⁻ ^a	1.726
SeO ₄ ²⁻ ^a	1.709
SeO ₄ ²⁻ ^b	1.634
HSeO ₄ ^{-b}	1.638*
H ₂ SeO ₄ ^b	1.642*
SeO ₃ ²⁻ ^b	1.691
HSeO ₃ ^{-b}	1.699*
H ₂ SeO ₃ ^b	1.700*

2.3 Comparison of oxo sulfur and oxo selenium anions

The internal central atom to oxygen distances in the ions X-O where X is S or Se increases as expected by the increase in ionic radius of X. We see that there is a decrease in the effectiveness as a structure maker where X is partially reduced this trend can be seen when studying the crystal data for hydrated Se crystals of decreasing oxidation state of the central atom. This trend fits well with the lower charge density in the anion and introducing a weaker lone-pair that the oxygen presents clearly affects the ability to

hydrogen bond atoms. The effective bonding distance and angles found for these systems are within the criteria for hydrogen bonding but the interaction is significantly weaker than the hydrogen bonds at the oxygen site. The orientation of the coordinating water molecules are not yet determined other than in a broad sense through some form of electrostatic ordering. Comparing the CN of the oxosulfur anions studied with the oxoselenium anions it is surprising to find the larger oxoselenium ions to have lower coordination which means that the lower CN cannot be explained by crowding. The selenate ion has lower coordination than the lower charge density selenite ion, this might be explainable by the mechanistic differences in symmetric vs asymmetric hydration respectively. Water coordination to the lone-pair of the central atom of selenite and sulfite is much weaker than that of the oxygens and in sulfite the exchange between the hydration sphere and bulk only takes place in cones along the central axis.

3 Conclusion

Comparing the oxosulfur and oxo selenium ions in the state +IV and +VI systems, there is a strong structural similarity in the structural transitions from higher oxidation state to lower, i.e the occurrence of dual distances for the central ion to water oxygens in the lower oxidation states not present in the higher oxidation state. This suggests similar behavior of hydration and looking at selenite- selenate it is expected that the behavior of the lower state has similar dynamics as the sulfite ion. It is also obvious that these anions all are weak structure makers, something that could be viewed as a possible trend where the ability to function as a structure maker is correlated to increased charge density and symmetric hydration of the anion. Furthermore it is reasonable to assume that the difference in charge density of the lone-pair on selenium and oxygen in the selenite ion will generate a similar difference in strength of the ion-water interactions as observed in the sulfite ion. This implies that there would be a similarly conical behavior in the hydration sphere of selenite as observed for sulfite in Paper I.

To summarize the asymmetric hydration observed generates a significantly different water exchange behavior between the hydration shell and bulk compared to symmetric systems and there is a need to develop tools which better describes the dynamics of asymmetric systems.

References

- Atkins, P. (2000). *The elements of physical chemistry*. 3. ed. Oxford: Oxford University Press. ISBN 9780198792901.
- Bakker, H. J. (2008). Structural dynamics of aqueous salt solutions. *Chemical Reviews* 108(4), 1456-1473.
- Huheey, J. (1993). *Inorganic chemistry : principles of structure and reactivity*. 4. ed. New York NY: HarperCollins College Publishers. ISBN 9780060429959.
- Kristiansson, O. & Lindgren, J. (1991). Infrared spectroscopic studies of concentrated aqueous electrolyte solutions. *The Journal of Physical Chemistry* 95(3), 1488-1493.
- Marcus, Y. (2009). Effect of Ions on the Structure of Water: Structure Making and Breaking. *Chemical Reviews* 109(3), 1346-1370.
- Nič, M., Jirát, J., Košata, B., Jenkins, A. & McNaught, A. (Eds.) (2009a). coordination entity. *IUPAC Compendium of Chemical Terminology*. 2.1.0. ed. Research Triangle Park, NC: IUPAC. ISBN 0-9678550-9-8.
- Nič, M., Jirát, J., Košata, B., Jenkins, A. & McNaught, A. (Eds.) (2009b). coordination number. *IUPAC Compendium of Chemical Terminology*. 2.1.0. ed. Research Triangle Park, NC: IUPAC. ISBN 0-9678550-9-8.
- Persson, I. (1984). *X-ray scattering on liquids, solutions, melts and noncrystalline solids*.
- Rode, B. M. & Hofer, T. S. (2006). How to access structure and dynamics of solutions: The capabilities of computational methods (Special Topic Article). *Pure and Applied Chemistry* 78(3), 525-539.
- Rode, B., Hofer, T., Randolf, B., Schwenk, C., Xenides, D. & Vchirawongkwin, V. (2006). Ab initio quantum mechanical charge field (QMCF) molecular dynamics: a QM/MM – MD procedure for accurate simulations of ions and complexes. *Theoretical Chemistry Accounts: Theory, Computation, and Modeling (Theoretica Chimica Acta)* 115(2), 77-85.

Acknowledgements

My Supervisor Professor Ingmar Person, for introducing me to the molecular marvels of hydrated anions and inorganic chemistry

My co-supervisor Professor Bernt Michael Rode, for the computational time and the warm welcome in Innsbruck

PhD Thomas Hofer for developing the ARD and helping me understand my data

PhD Len Herald Lim for developing the S-lightly I-ntelligent P-arser tool which made a lot of the analysis work just breeze by

PhD Andreas Pribil for helping me initialize the data run and providing the water box

PhD Mats Petterson for being a solid friend and always willing to listen to my ramblings on the science and life in general

Jonas Söderberg for being a good friend and for making me eat lunch

All my colleagues in Innsbruck

All my colleagues in Uppsala especially Gunnar Almquist, Johan Mhåler and Berndt Andersson

To the roleplaying gang for distracting me in a most wonderful way "Det börjar bli mörkt nu, eller skulle i alla fall bli det om ni inte alla såg i mörker." och "Det finns inga Ugglebjörnar!"

Friends and family which makes even the most stressed times bearable

Finally to my wonderful and fantastic wife Sandra without whom I would be completely lost, I love you



I



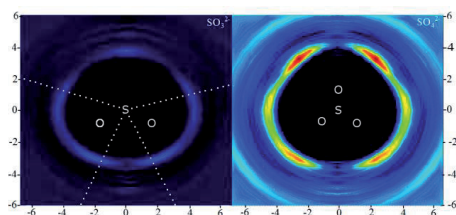
On the Structure and Dynamics of the Hydrated Sulfite Ion in Aqueous Solution – An *ab initio* QMCF MD Simulation and Large Angle X-ray Scattering Study

Lars Eklund,^a Tomas S. Hofer,^b Andreas Pribill,^b Bernd M. Rode^b and Ingmar Persson^{a,*}

^a Department of Chemistry, Swedish University of Agricultural Sciences, P.O.Box 7015, SE-750 07 Uppsala, Sweden.

^b Theoretical Chemistry Division, Institute of General, Inorganic and Theoretical Chemistry, University of Innsbruck, Innrain 52a, A-6020 Innsbruck, Austria,

Graphical Abstract



Synopsis

The sulfite ion has an asymmetric hydration sphere with three water molecules hydrogen bound to each of the sulfite oxygen, and with 3-4 water molecules clustered outside the lone electron-pair. An angular radial distribution analysis has shown that the water exchange only takes place between the water molecules clustered outside the lone electron-pair and the aqueous bulk. This is opposite to the hydrated sulfate ion where the three water molecules, symmetrically hydrogen bound to each sulfate oxygen, exchange directly with the aqueous bulk.

Abstract

Theoretical *ab initio* quantum mechanical charge field molecular dynamics (QMCF MD) formalism has been applied in conjunction with experimental large angle X-ray scattering to study the structure and dynamics of the hydrated sulfite ion in aqueous solution. The results show that there is a considerable effect of the lone electron-pair on sulfur concerning structure and dynamics in comparison with the sulfate ion with higher oxidation number and symmetry of the hydration shell. The S-O bond distance in the hydrated sulfite ion has been determined to 1.53(1) Å by both methods. The hydrogen bonds between the three water molecules bound to each sulfite oxygen are only slightly stronger than in bulk water, and the sulfite ion can therefore be regarded as a weak structure maker. The water exchange rate is somewhat slower for the sulfite ion than for the sulfate ion, $\tau_{0.5} = 3.2$ and 2.6 ps, respectively. An even more striking observation in the angular radial distribution (ARD) functions is that for sulfite ion the water exchange takes place in close vicinity of the lone electron-pair directed at its sides, while in principle no water exchange did take place of the water molecules hydrogen bound to sulfite oxygens during the simulation time. On the other hand, for the hydrated sulfate ion in aqueous solution one can clearly see from the ARD that the distribution of exchange events is symmetrical around the entire hydration sphere.

Introduction

The hydration of anions is essential due to its immense importance in chemical and biological reactions. When a reaction takes place in an aqueous solution the reaction is influenced by the exchange between the reactants and the solvent molecules. The effects of hydration is however not limited to the local effect of interactions with the hydrated ion itself but also with the macroscopic properties of the solution. Studies of partially reduced hydrated anions such as sulfite have been scarce, especially the effects comparing anions with different hydration symmetry.

Sulfite plays a major role in the production of many chemicals among the most important is the production of sulfuric acid. There is a large number of registered patents involving the sulfite ion in aqueous systems.¹ Clearly, knowledge of the structure and dynamics of the hydrated sulfite ion in aqueous solution is vital in many aspects, but poorly studied so far. The use of theoretical simulations in combination with experimental structure determination is particularly powerful as it gives complementary information from different starting points at different timescales. The time average structure found with the X-ray scattering can verify the theoretical model with the lowest energy state in the simulation and the simulation gives information about short time events at the sub femto-second level unattainable by present experimental methods. This information is especially valuable in systems with weak interactions since these are particularly affected by high exchange rates.

The aim of the present study is to determine the structure and dynamics of the hydrated sulfite ion in aqueous solution by both experimental and theoretical methods. The sulfite ion has a lone electron-pair on the central sulfur atom which is expected to influence both structure and the dynamics in comparison to the symmetric sulfate ion.² The sulfite oxygens have three free electron-pairs, which is of importance for the hydrogen bonding acceptor properties. The structure of the hydrated sulfite ion in aqueous solution will be discussed in terms of how strong the hydrogen bonds of the hydrating water molecules are in comparison with the strength of hydrogen bonds in the aqueous bulk. Thus, what is the structural relationship of the thermodynamically determined properties in regard to the structure making or breaking properties^{3,4}. Comparisons are made with the sulfate ion to study the effects of decreasing the symmetry of the hydration shell of hydrated

oxosulfur anions.

Experimental

Chemicals. Sodium sulfite, Na₂SO₃ (pro analysis, Merck), and sodium hydroxide, NaOH (reagent grade, Sigma-Aldrich), were used without further purification.

Solution. The solution for the LAXS experiment was prepared by dissolving a weighed amount of sodium sulfite in deionized Milli Q filtered water, and pH was adjusted to 12.0 by addition of a small amount of sodium hydroxide to a final concentration of 1.5987 mol·dm⁻³, and a density of 1190.4 g/L. The water concentration in this solution was 54.892 mol·dm⁻³.

LAXS. The scattering of MoK α X-ray radiation, $\lambda=0.7107$ Å, from the free surface of the aqueous sodium sulfite solution was measured in a large angle Θ - Θ goniometer described elsewhere.⁵ The solution was contained in a teflon cup filled until a positive meniscus was observed generating a flat surface in the irradiated region. The container was placed inside an air-tight radiation shield with beryllium windows. The scattered radiation was monochromatised using a LiF(200) single crystal focusing monochromator. The scattering was determined at 446 angles in the angle range of $0.5 < \Theta < 65^\circ$, where the scattering angle is 2Θ . At each angle 100,000 X-ray quanta were counted, and the entire angle range was scanned twice corresponding to a statistical error of about 0.3 %. The divergence of the x-rays was defined through combination of divergence-collecting-focal slits of $\frac{1}{4}^\circ$ - $\frac{1}{2}^\circ$ -0.2 mm and 1° - 2° -0.2 mm. Three different Θ -regions were scanned to get a suitable counting rate and change in angle, with overlapping regions to enable scaling of the data. The data collection and treatment are described in detail elsewhere.⁵ All data treatment was carried out using the KURVLR program,⁶ and the structural parameters in the theoretical model were refined by minimizing $U = w(s)\sum s^2 [i_{\text{exp}}(s) - i_{\text{calc}}(s)]^2$ using the STEPLR program.^{7,8} The experimental data were normalized to a stoichiometric unit containing one sulfur atom, using the scattering factors f for neutral atoms, including corrections for anomalous dispersion, $\Delta f'$ and $\Delta f''$,⁹ Compton scattering^{10,11} and multiple scattering events. The latter is especially important as it plays a significant role since the molar absorption coefficient of the solution was low, $\mu = 2.113$ cm⁻¹.

QM/MD through QMCF. In this study the simulation was divided into two steps. In the initial step the system was equilibrated for 6.5 ps, where the system momentum, energy and temperature were closely monitored, and the molecular geometry was analyzed each 0.8 ps. After this initial equilibrium simulation a data sampling was started which lasted for 14 ps. A step size of 0.2 fs was used in both the equilibrium and sampling phase. The flexible BJH-CF2 water model¹² was used enabling the study of explicit hydrogen motion of the water molecule. The simulation of the hydrated sulfite ion in aqueous solution used *ab initio* quantum mechanical charge field molecular dynamics (QMCF).¹³ The QMCF approach employs the Hartree-Fock (HF) level to evaluate the intermolecular forces in the quantum mechanical region containing the solute molecule and two layers of hydration. In the past the HF approach was successfully employed in QMCF MD simulation studies of hydrated sulphate.³ During the computation of the interaction between particles in the QM and MM regions, the QM region is further separated into an inner core and outer layer region. Particles located in the layer zone interact with the MM atoms via a Coulombic and a non-Coulombic term. Due to the large distance between particles in the core region and the QM/MM interface, atoms in the core region interact with particles in the MM region only via a Coulombic potential as the non-Coulombic contribution is negligible¹⁴. This is of particular advantage in the case of complex solute species such as the sulfite ion. The QM core radius was set to 4.5 Å, the total QM radius was 7.2 Å. The QM region contained roughly 45 water molecules throughout the simulation. The simulation box used was the same as reported elsewhere.¹⁵ The phosphate anion was replaced by sulfite which had been structure optimized together with 10 water molecules using Gaussian.¹⁶ A periodic boundary box with the edge length of 31.4 Å was used containing 1000 water molecules, with a density of 0.997 g·cm⁻³ at the target temperature 298 K, and thermostated via the Berendsen weak coupling algorithm.¹⁷ The reaction field approach was employed to account for the error associated to the application of a Coulombic cutoff set to 12.0 Å. The simulation was carried out using the DZP -dunning basis sets^{18,19} and TURBOMOLE 6.00.²⁰

Analysis methods of the QMCF simulation. Radial distribution functions (RDFs) with different

kind of atoms as origin were used for the radial population analyses. This can be expressed as $g(r) = V/N^2 \langle n(r, \Delta r) \rangle_M / 4\pi r^2 \Delta r$. The main difference between an experimental RDF expressed as $D(r) - 4\pi r^2 \rho_o$ from scattering experiment and the RDF generated from a simulation is that in the first case the center of increased electron density in space is regarded as atoms and the distance between such centra as an atom-atom distance as determined in the experiment, while in the simulations the position of the atom centres is known and the distribution of the atoms is calculated.

By constraining the analysis of the RDF within overlapping conical regions with a central vector defined as the sum of the three sulfur bound oxygens, the distribution around the ion can be probed as a function of distance and angle, a so called angular radial distribution (ARD) function which is dependent of the distance from a given center $D(r, \alpha)$. In this analysis of the simulation α was 22.5° . By giving a radial criteria a population analysis inside a given band can be made, or sphere of affected waters. If this is done over the entire simulation time the coordination number distribution over time can be calculated. The mean residence time, MRT, τ_i , was calculated in a radial sphere of 2 to 5 Å from the central sulfur atom. The MRT is the time a given atom spends inside a given region over the entire simulation. The exchange rate analysis which counts the number of crossings of the region border is related to this analysis. By counting the number of exchange events with a residence time of at least 0.0 and 0.5 ps defines the sustainability of exchange $S_{ex} = N_{ex}^{0.5} / N_{ex}^0$ and is related to the strength of the interactions between the ligand and central ion. The higher S_{ex} value the lower the probability of exchange given the same ligand availability. This means stronger interactions with the ligands in that coordination shell. Density plots were created by population analysis in a rotating periodic box centered on the sulfur within the simulation box. In order to analyse the angular distributions of $O_w \cdots S \cdots O_w$ the system was hemispherically partitioned with a plane perpendicular to the dipole moment of the sulfite ion and passing through the sulfur atom, Figure 1. The angular distribution functions could then be separated based on in which hemisphere the oxygen resides. Further studies on the sulfur oxygen, O_{SO_3} , water oxygen, O_w , was done through analysis of the tilt of the $O_{SO_3} \cdots O_w$ vector, here denoted

OO, with respect to the plane of the water molecule. The angle between the dipole vector of the water molecules and **OO** was also analysed. For both the tilt and the dipole calculations a sphere of 3 Å around the O_{SO_3} was probed. The tilt shows the out- of- plane angle of the **OO** irrespectively of the in-plane orientation of the water, and the dipole angle takes in consideration the in plane movement of the waters dipole orientation. These two analysis methods thereby describe the orientations of waters in the hydration shell as relevant for hydrogen bonding to the O_{SO_3} .

Results and Discussion

Large Angle X-ray scattering

The experimental radial distribution function RDF for the aqueous sulfite solution shows four peaks at 1.5, 3.0, 3.7 and 4.2 Å, Figure 2. The peak at 1.5 Å corresponds to the mean S-O bond distance in the sulfite ion, and has been refined to 1.53(1) Å. This S-O bond distance is slightly longer than in the solid structures of sulfite salts only electrostatically interacting with monovalent counter ions, mean 1.513 Å, but it is identical to the S-O bond distances observed in salts where the metal ion has a complete hydration shell allowing hydrogen bonding to the sulfite ion, mean 1.534, Table S1. Furthermore, in the latter salts each sulfite oxygen atom accepts hydrogen bonds to three neighboring water molecules. This shows that the hydrogen bonding to the sulfite oxygens increases the mean S-O bond length with 0.015-0.02 Å as it has been found in similar systems.³ The main peak at 3.0 Å corresponds to the $O_w \cdots O_w$ distances in aqueous bulk, $O_w \cdots O_w$, and between sulfite oxygens and hydrating water molecules, $O_{SO_3} \cdots O_w$. It has not been possible to separate these distances due to their similar values, and the mean value of these distances has been refined to 2.878(4) Å. This is just slightly shorter than the mean $O_w \cdots O_w$ distance in aqueous solutions, 2.89 Å.^{3,21} This strongly indicates that the $O_{SO_3} \cdots O_w$ distances are slightly shorter and the hydrogen bonding slightly stronger than in the aqueous bulk. The weak peaks at 3.7 and 4.2 Å are assigned to $S \cdots O_w$ distances to the water oxygens hydrogen bonding to sulfite and the water molecules outside the lone electron-pair, respectively. These have been refined to 3.68(3) and 4.16(4) Å, respectively. The $S \cdots O_w$ distance corresponds to a tetrahedral $S-O_{SO_3} \cdots O_w$ angle strongly supporting that three

water molecules hydrogen bond to each sulfite oxygen, as also found in the solid state, see above, and in the QMCF simulation, see details in next section. The longer $S \cdots O_w$ distance to the water molecules is assumed to be located outside the lone electron-pair shows that the hydration shell around the sulfite ion is irregular and that the lone electron-pair takes up significant space. The structure of the hydrated sodium ion is in good agreement with previous studies.³ The structure parameters of the aqueous sodium sulfite solution studied are summarized in Table 1.

QMCF Simulations

Radial distribution functions, RDFs, of individual atom-atom distances were calculated from the final result of the QMCF/MD simulation, Figures 3a-e, the distances determined in the hydrated sulfite ion in the simulation are compared with those from the LAXS data in Table 1. Each sulfite oxygen bind three water molecules through hydrogen bonding. The peaks at 3.73 and 4.11 Å with FWHM values of 0.530 and 0.370 Å, respectively, correspond to the mean $S \cdots O_{SO3p}$ and $S \cdots O_{SO3d}$ distances, Figure 3d1; SO3p and SO3d refer to water molecules interacting with sulfite oxygens and the water molecules outside the lone electron-pair, respectively. However, these distances are influenced by long-range $S \cdots H$ and $O \cdots H$ interactions and the given values are therefore somewhat uncertain. By studying the RDF of the $S \cdots H$ distances in detail, Figures 3b and 3b1, the $S \cdots H_{SO3p1}$ is determined to 2.79 Å and $S \cdots H_{SO3d}$ 2.99 Å. There is a third distance in the detailed distinguishable in the $S \cdots H$ plot at 4.2 Å which corresponds to H_{SO3p2} . H_{SO3p1} and H_{SO3p2} represent hydrogens closer to the sulfur than the water oxygen to which it is bound (SO3p1) and further away (SO3p2). H_{SO3d} is hydrogen bound to water molecules in the vicinity of the sulfur lone pair. Contrary to the experimental LAXS data the RDF from simulation is built up by separable pair functions and can therefore be resolved, for the $O_{SO3} \cdots O_w$ and $O_w \cdots O_w$, with the distances at 2.77 Å and 2.83 Å respectively, Figure 3e, in dilute solution. The contribution of the hydration sphere to the total interactions is small, in this simulation about 300 times less than the bulk contribution. The contribution increases with concentration of the solute of course and at the concentrations used in the LAXS measurement it becomes quite significant. The difference between oxygen oxygen distances for bulkwater ($O_w \cdots O_w$) and the waters of the first hydration shell ($O_{SO3} \cdots O_w$) is 0.06 Å

which is consistent with the geometries of the LAXS measurements. The S-O bond distance obtained from the QMCF simulation, Figure 3b, is in full agreement with the experimental LAXS study, as well as the distances to the proximal and distal waters Tables 1 and 2. The $S\cdots H$ and $O_{\text{sulfite}}\cdots H$ distances, Figures 3c and 3d, shows shorter distances than the S-O and $O_{\text{sulfite}}\cdots O_{\text{aq}}$ distances, Figure 3e, which show that the orientation of the hydrogens is towards the anion.

The distribution of coordination number (CN) is shown in Figure 4 giving an average of 12.5 showing the presence of only one coordination sphere of water molecules different from those in the bulk, which is in full agreement with the observations made by LAXS, see above.

An ARD function was constructed in order to study the structure and dynamics of the hydrated sulfite in more detail, Figure 5. Figure 6, left panel, shows that there are areas outside of the hydration sphere that show zero occupation of oxygen throughout the duration of the simulation time except for a small area diametrically to the lone pair. This means that apart from a small exchange diametrically across from the sulfur lone-pair no exchange between the bulk water molecules and the water molecules hydrogen bound to the sulfite oxygen takes place. In principle all water exchange is directed through a cone of water molecules outside the lone electron pair. This means that a water exchange event of the water hydrogen bound to sulfite oxygen requires that it must be transferred from a point in the hydration sphere and across the spherical boundary. If $D(r,\alpha)_{\text{sulfur-oxygen}} = 0$ for a given r,α on the spherical boundary, no trajectory may have passed through that coordinate and no exchange have taken place along that trajectory. The ARD of the hydrated sulfate ion, SO_4^{2-} (aq), Figure 6 right panel, in aqueous solution clearly show that sulfate has a symmetric hydration sphere with water exchange taking place uniformly over the entire sphere. If we compare this with the sulfite ion which has an asymmetrical behavior as discussed above, we can conclude that a centrosymmetric analysis, such as the MRT analysis, will not give the correct picture of the exchange flux mechanism.

The angular density functions(ADF) of the sulfite ion in aqueous solution of $O_{\text{SO}_3}-S\cdots O_w$, Figure 7. For the oxygens O_B , interacting with the sulfite oxygens, O_{SO_3} there are three distinct maxima at 36, 77, 130 , Figure 7 c. In contrast the O_A oxygens interacting with the sulfur only has a minor distinctive peak at 48 degrees and then a broad band covering the mayor part of the angular

space, Figure 7 b. This implicates that there is a higher order of the water molecules clustered around the O_{SO_3} than for the water molecules clustered outside the lone electron pair on the sulfur atom. Examining the tilt for the sulfite $O_{SO_3} \cdots O_w$ bond Figure 8a we can see that there is a slight out-of-plane tilt of the angle ± 30 degrees which means that the orientation of the bond to the O_{SO_3} is mostly in-plane-oriented which is consistent with hydrogen bonding of the water molecules. Furthermore the dipole angle of sulfite oxygens to water, Figure 8b, the orientation is limited to three peaks at 30, 135 and 155. The 30 degree peak is consistent with waters in the transition area and the other two peaks represent an orientation consistent with hydrogen bonding.

A comparison of first shell MRT for sulfate, phosphate, sulfite and bulk water at Hartree-Fock level is presented in Table 2. The residence time of the first shell of water molecules of the hydrated sulfite ion is, 3.2 ps, which is intermediate of the sulfate ion, 2.6 ps, and the phosphate ion, 3.9 ps,^{2,3,15} By calculating the sustainability coefficient, which is the number of exchange events longer than 0.5 ps over the total number of events, $S_{ex} = N^{0.5}_{ex}/N^{0.0}_{ex} = 0.171$. For pure water^{22,23} $S_{ex} = 0.089$ making the hydration shell about twice as stable as that of pure water. This structure making ability is concurrent with previous reports calculated on the free energy of hydrogen bonds based on the viscosity coefficients.^{4,5} The MRT and the S_{ex} are inherently symmetric and the behavior of the sulfite ions hydration is asymmetric. This generates a problem when comparing symmetrically behaving ions with asymmetric ones since almost all flux water exchange takes place through the water molecules clustered outside the lone pair side and almost no exchange takes place outside this region. This means that the rate determining step might not be the exchange between hydration shell and bulk but rather the transfer of water molecules inside the hydration shell, while for a symmetric system, such as hydration of sulfate ion, the water exchange mechanism takes place directly between a water molecule hydrogen bound to the sulfate oxygen and a bulk water molecule.

Conclusions

The sulfite ion has an asymmetric hydration sphere with three water molecules hydrogen bound to each sulfite of the oxygen, and with 3-4 water molecules clustered outside the lone electron-pair. The spatial density plot, Figure 9, illustrate that there is a considerable asymmetry in the hydration sphere generated by the lone pair. An angular radial distribution (ARD) analysis did show that the

water exchange rate of the water molecules hydrogen bound to sulfite oxygens is very slow within the time of the simulation, 20 ps, except for a minor exchange taking place diametrically opposite to the lone electron pair. The water exchange of hydrated water molecules takes in principle only place between the water molecules clustered outside the lone electron-pair and the aqueous bulk. The water molecules hydrogen bound to the sulfite oxygens can be transferred to the region of the lone electron-pair, and there be exchanged. On the other hand, in the hydrated sulfate ion, with higher symmetry, the water molecules, hydrogen bound in the very same way as in the sulfite ion, are readily exchanged directed with surrounding bulk water molecules in a completely different mechanism.

Acknowledgments

We gratefully acknowledge the financial support from the Swedish Research Council and the Austrian Science Foundation.

Supporting Information Available: Additional information as noted in the text and a complete reference 16. This material is available free of charge via the Internet at <http://pubs.acs.org>.

References

- (1) The United States Patent and Trademark Office (USPTO). <http://www.uspto.gov/index.jsp> (accessed Dec 3, 2010)
- (2) Vchirawongkwin, V.; Rode, B. M.; Persson, I. *J. Phys. Chem. B* **2007**, *111*, 4150-4155.
- (3) Marcus, Y. *J. Solution Chem.* **1994**, *23*, 831-848.
- (4) Marcus, Y. *Chem. Rev.* **2009**, *109*, 1346-1370.
- (5) Stålhandske, C. M. V.; Persson, I.; Sandström, M.; Kamienska-Piotrowicz, E. *Inorg. Chem.* **1997**, *36*, 3174-3182.
- (6) Johansson, G.; Sandström, M. *Chem. Scr.* **1973**, *4*, 195-198.
- (7) Molund, M.; Persson, I. *Chem. Scr.* **1985**, *25*, 197-197.
- (8) Chandler, J. P. *Behavioral Science* **1969**, *14*, 81-82.
- (9) Wilson, A. J. C., Ed. *International Tables for Crystallography*; Kluwer Academic Publishers: Dordrecht, The Netherlands, 1995; Vol. C.
- (10) Cromer, D. T. *J. Chem. Phys.* **1969**, *50*, 4857-4879.
- (11) Cromer, D. T. *J. Chem. Phys.* **1967**, *47*, 1892-1893.
- (12) Bopp, P.; Jancsó, G.; Heinzinger, K. *Chem. Phys. Lett.* **1983**, *98*, 129-133.
- (13) Rode, B.; Hofer, T.; Randolph, B.; Schwenk, C.; Xenides, D.; Vchirawongkwin, V. *Theoretical Chemistry Accounts: Theory, Computation, and Modeling (Theor. Chim. Acta)* **2006**, *115*, 77-85.
- (14) Hofer, T. S.; Pribil, A. B.; Randolph, B. R.; Rode, B. M. In *Combining Quantum Mechanics and Molecular Mechanics. Some Recent Progresses in QM/MM Methods*; Academic Press, 2010; Vol. 59, pp. 213-246.
- (15) Pribil, A. B.; Hofer, T. S.; Randolph, B. R.; Rode, B. M. *J. Comput. Chem.* **2008**, *29*, 2330-2334.
- (16) Frisch, M. J. et al. *Gaussian 03, Revision E.01*.
- (17) Berendsen, H. J. C.; Grigera, J. R.; Straatsma, T. P. *J. Phys. Chem.* **1987**, *91*, 6269-6271.
- (18) Dunning, T. H. *J. Chem. Phys.* **1970**, *53*, 2823-2833.
- (19) Magnusson, E.; Schaefer, H. F. *J. Chem. Phys.* **1985**, *83*, 5721-5726.
- (20) Ahlrichs, R.; Bär, M.; Häser, M.; Horn, H.; Kölmel, C. ; *Chem. Phys. Lett.* **1989**, *162*, 165-169.
- (21) Torapava, N.; Persson, I.; Eriksson, L.; Lundberg, D. *Inorg. Chem.* **2009**, *48*, 11712-11723.
- (22) Hofer, T. S.; Tran, H. T.; Schwenk, C. F.; Rode, B. M. *J. Comput. Chem.* **2004**, *25*, 211-217.
- (23) Xenides, D.; Randolph, B. R.; Rode, B. M. *J. Chem. Phys.* **2005**, *122*, 174506.

Table 1. The distances determined for the different model atom complexes in LAXS experiments followed by the center and fwhh of the analytical peaks found in RDF from simulation.

Complex	Distance(Å)	fwhh	Method
S-O _{SO3}	1.53	0.128	LAXS
S··O _w	3.68	0.219	
S··O _{ip}	4.16	0.232	
water(O _w ··O _w)	2.878	0.210	
Na··O _w	2.407	0.224	
O-H	0.98	0.058	QMCF
S-O _{SO3}	1.53	0.074	
Bulk water O _w ··H	1.921	0.418	
water(O _w ··O _w)	2.828	0.299	
O _{SO3} ··O _w	2.770	0.340	
S··O _w	3.73	0.530	
S··O _{ip}	4.11	0.370	

Table 2. Mean residence times, MRTs, and the sustainability coefficients, S_{ex} , of water molecules in the hydrated sulfite, sulfate, phosphate ions and in bulk water from simulations on HF theory level.

Solvated ion	$\tau_{0.5}$	$N_{ex}^{0.5}$	$N_{ex}^{0.0}$	$1/S_{ex}$	Reference
Sulfite	3.2	59	346	5.9	This work
Sulfate	2.6	54	399	7.4	15
Phosphate	3.9	42	132	3.1	10
Bulk water	1.7	24	269	11.2	16

Legends to Figures

Figure 1. Describing the hemispherical portioning of water oxygens based on the dipole vector of the sulfite ion in aqueous solution

Figure 2. LAXS. (a) The individual peak shapes for all contributing species in the 1.5987 mol·dm⁻³ aqueous solution of sodium sulfite: the hydrated sulfite ion (orange line), the hydrated sodium ion (brown line), and aqueous bulk (green line). (b) Experimental $D(r) - 4\pi^2\rho_o$ (black line); model (red line), the modelled distances are given in table 1; difference (blue line). (c) Reduced LAXS intensity function, $s \cdot i_{\text{exp}}(s)$ (black line); model $s \cdot i_{\text{calc}}(s)$ (red line).

Figure 3. RDF's constructed from simulation data, a) linear summation of b)-e), b) S···H distances, c) O-H distances, d) S-O distances, the gray help lines shows $N=3$ and 12 which corresponds to ionic oxygens and coordinated oxygens, e) O···O. Subplots b.1) to e.1) show the interesting regions in more detail. In e.1) three different contributions red, blue and green representing total O···O, O_w···O_w and O_{SO3}···O_w respectively, the O_{SO3}···O_w curve (green line) is scaled 300 times.

Figure 4 CND, coordination number distribution. The CN numbers calculated from mean residence time at the HF level, The HF level always over estimates CN and the average CN 12.48 well agrees with the experimental value.

Figure 5. Contour plots of sulfur centered Angular Radial Distribution (ARD) functions, showing oxygens top left, hydrogen top right, and superimposed image. The superimposed image shows that the hydrogens of coordinated waters are oriented inwards, and the intensity of the path of exchange can be seen as dark blue intensity indicating zero in the normalized distribution function, i.e. no atoms are encountered, while brighter colors represents a non zero value.

Figure 6 Mesh plots viewed along the z axis showing water oxygen occupancy of sulfite, sulfate ion. The occupancy of a given angle, distance pair is given by intensity of the colors ranging from no occupancy, black, low medium occupancy, blue, to high occupancy yellow or red. The zero points are equal in intensity, the zero-point alignment shows the difference in transportation properties as one can determine which regions contain no exchange events

Figure 7. ADF:s, angular distribution functions, The Angular distribution over the simulation for the angle between the vectors as described by the figures adjacent to each curve for case a,b and c. The ADF:s show that there is a preferred region of occupancy for water molecules in the first hydration shell.

Figure 8. The tilt, out of plane angle of the $\mathbf{O}_s\mathbf{O}_w$ vector, show that there is two preferred angle ranges 30° out of plane on both sides of the plane and the Θ , angle of dipole moment vector and the $\mathbf{O}_s\mathbf{O}_w$ vector, show preference of 4 angular states during a time average for the water molecules over the simulation.

Figure 9. Density plots generated using a rotating box and fixed axes. The density plot illustrates the cavity created in the solution around the sulfite ion

Figure 1

Hemispherical partitioning of the system: according to SO_3^{2-} dipole vector

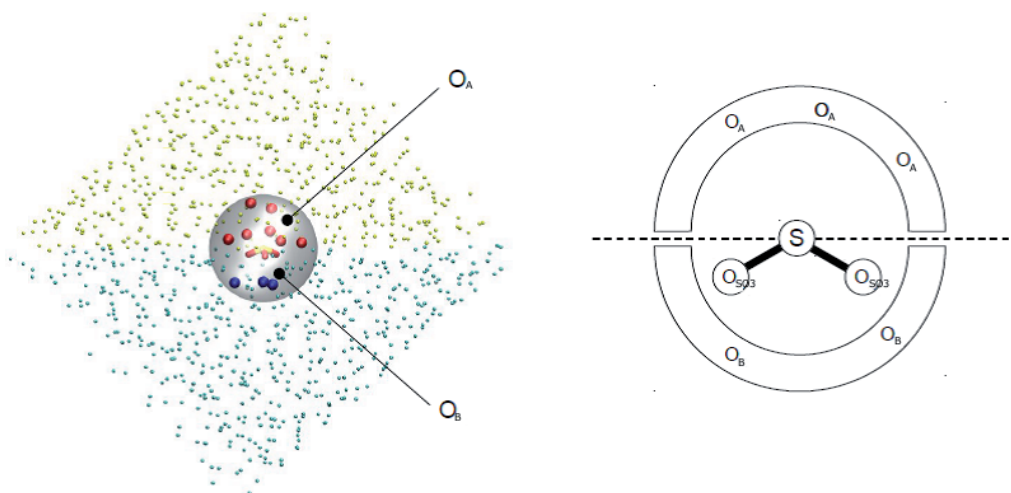


Figure 2

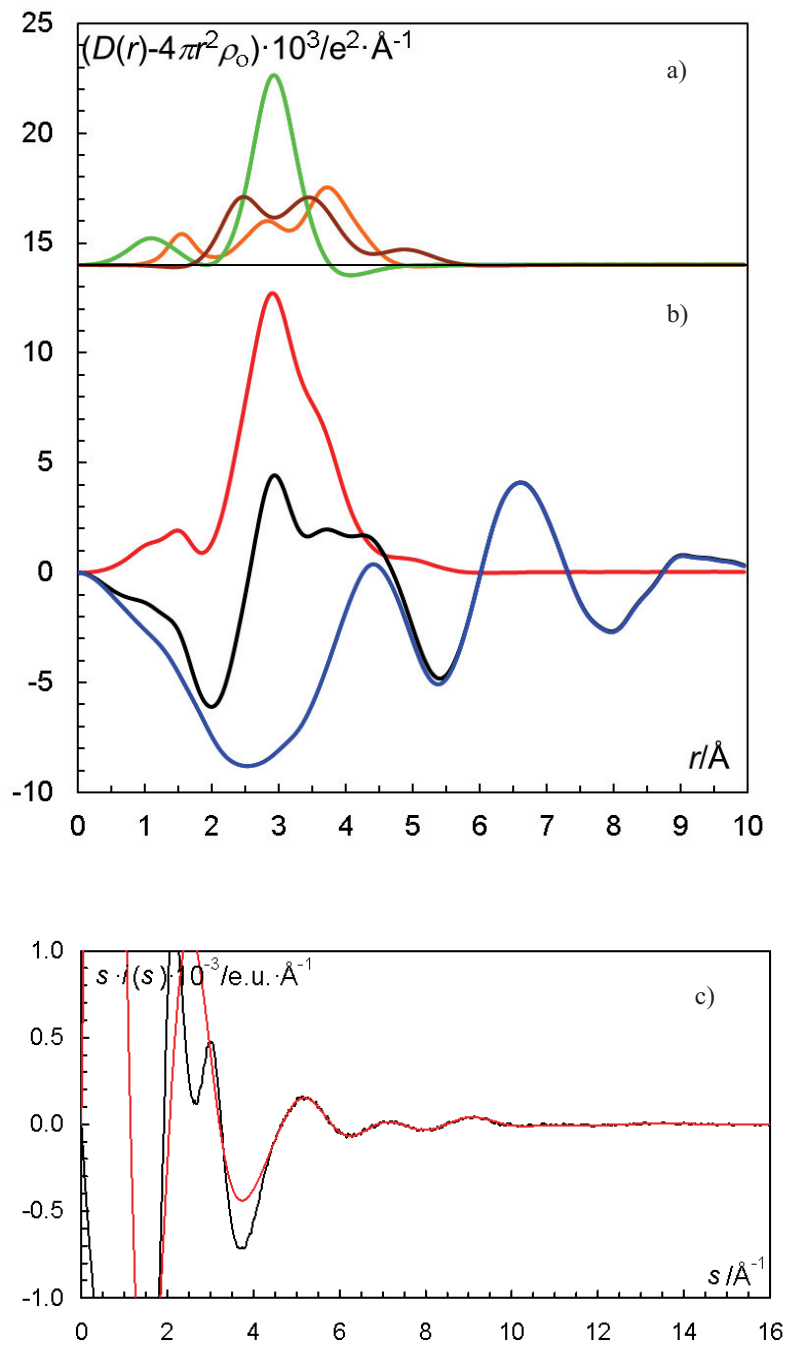


Figure 3

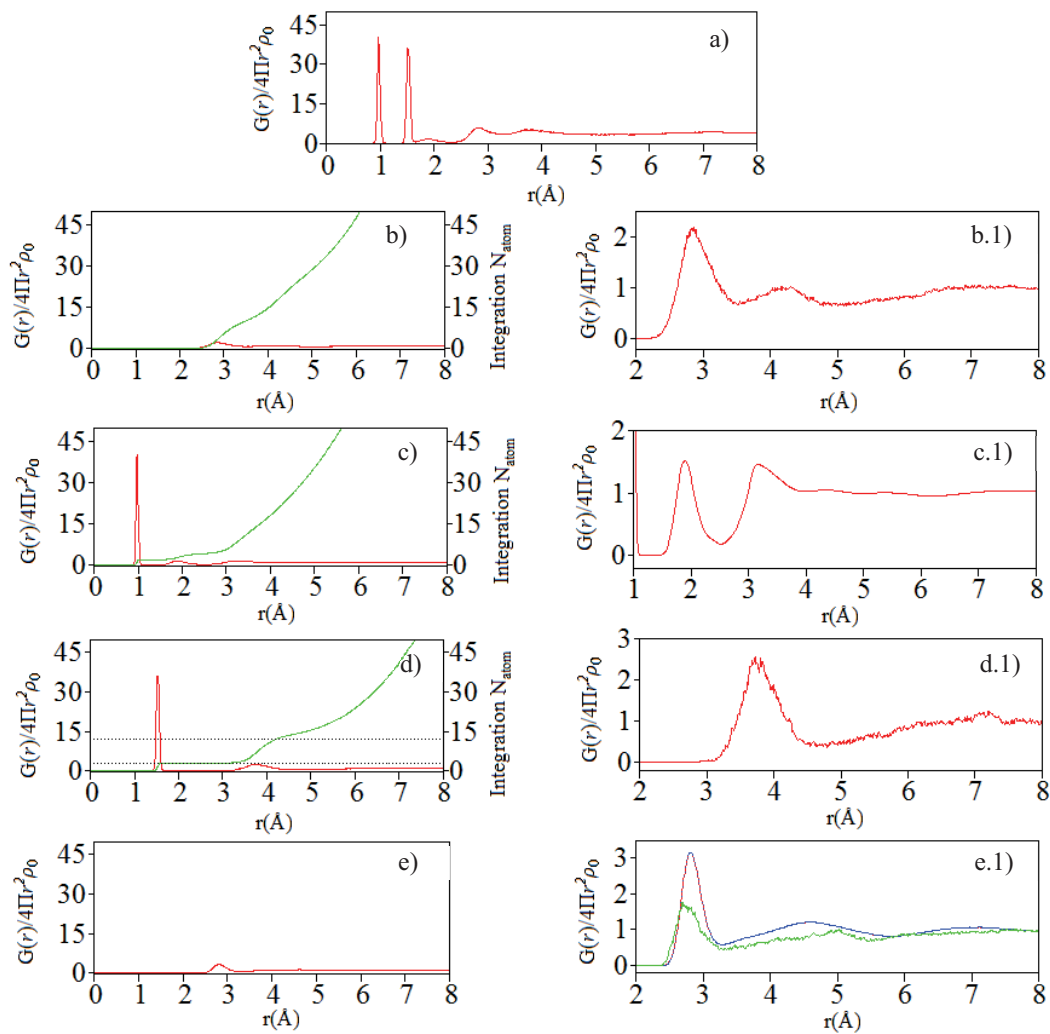


Figure 4

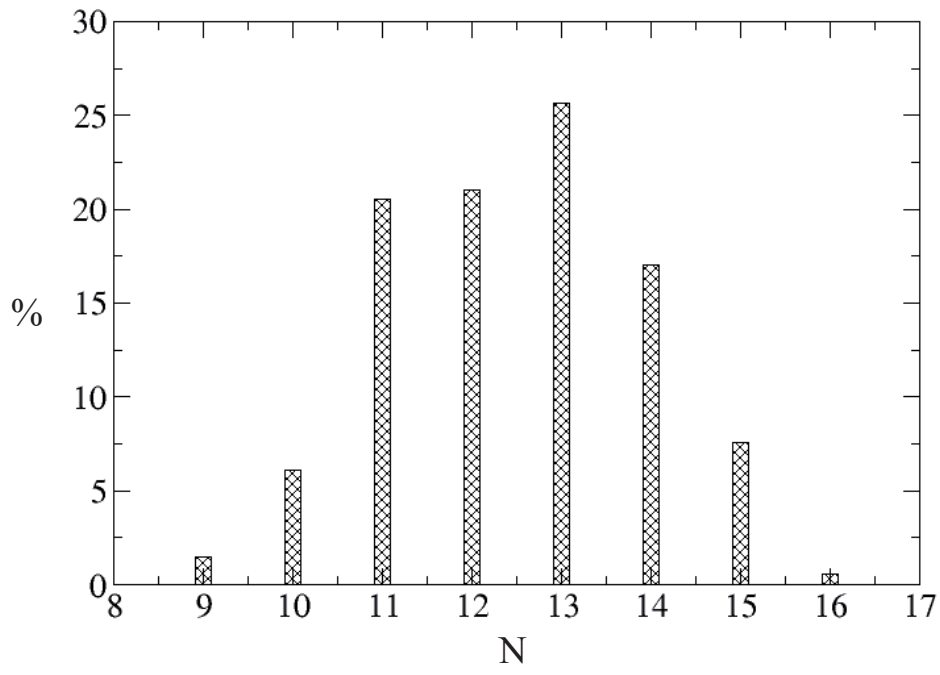


Figure 5

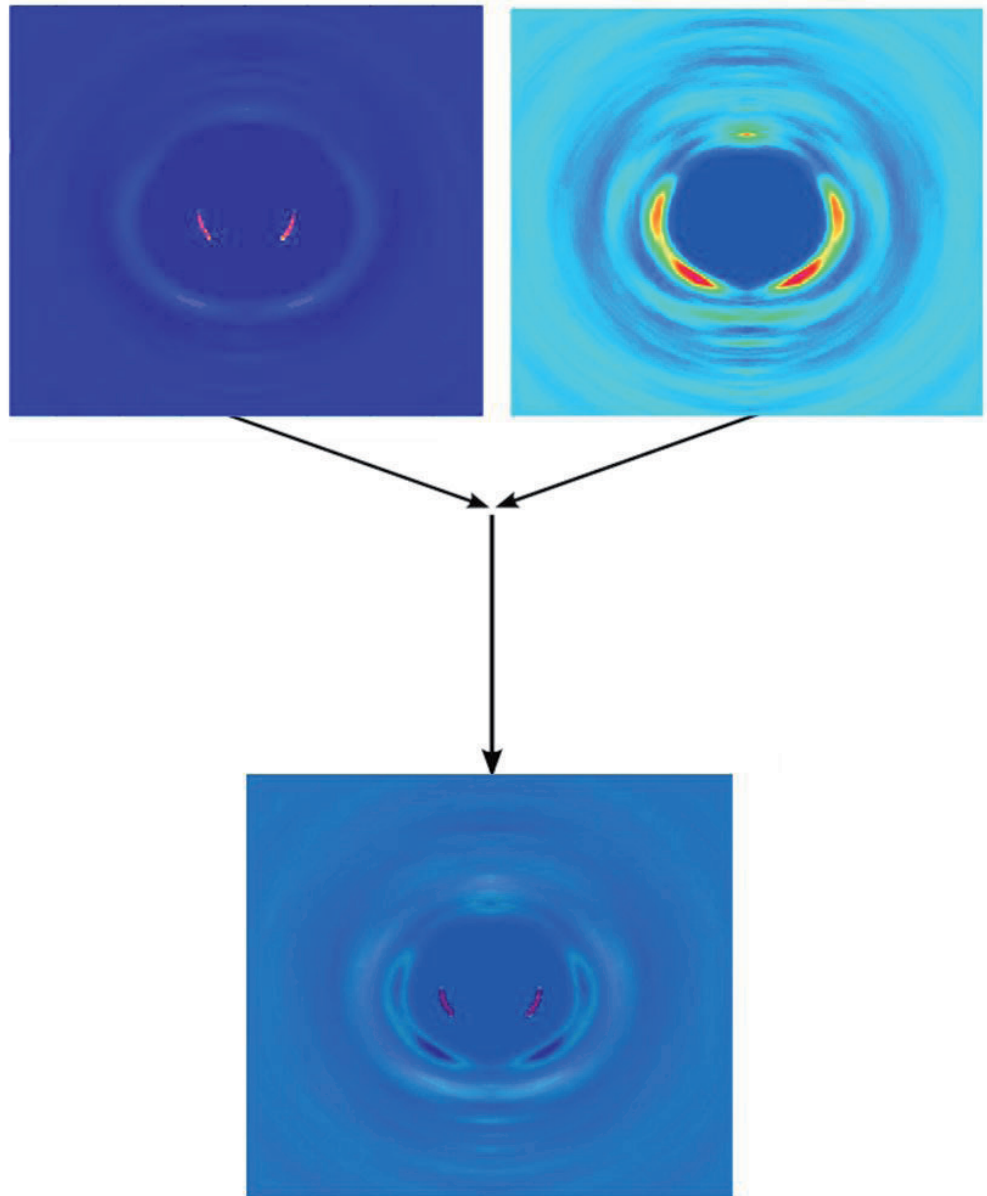


Figure 6

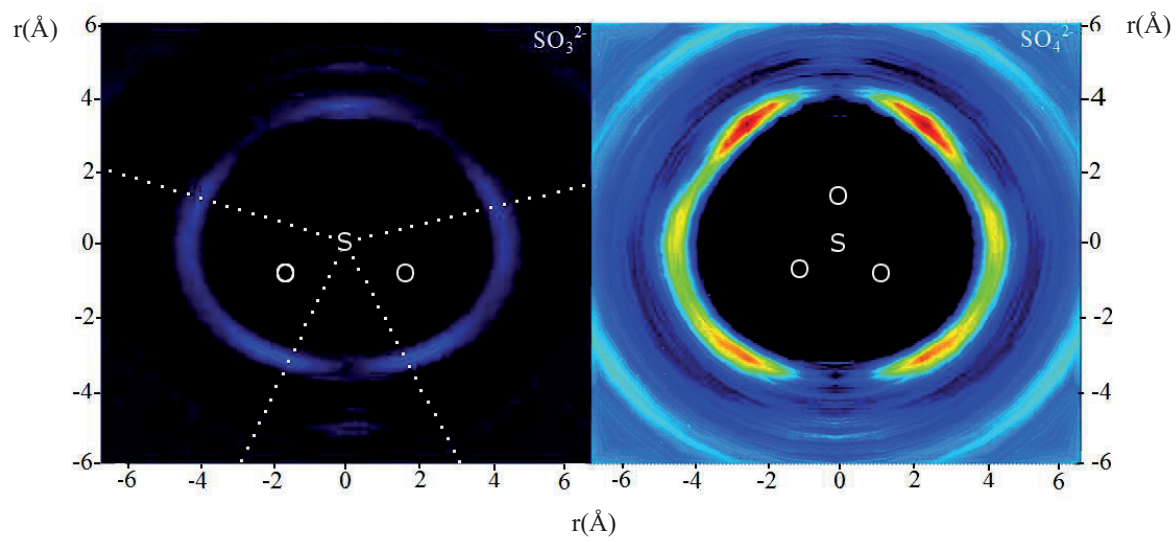


Figure 7

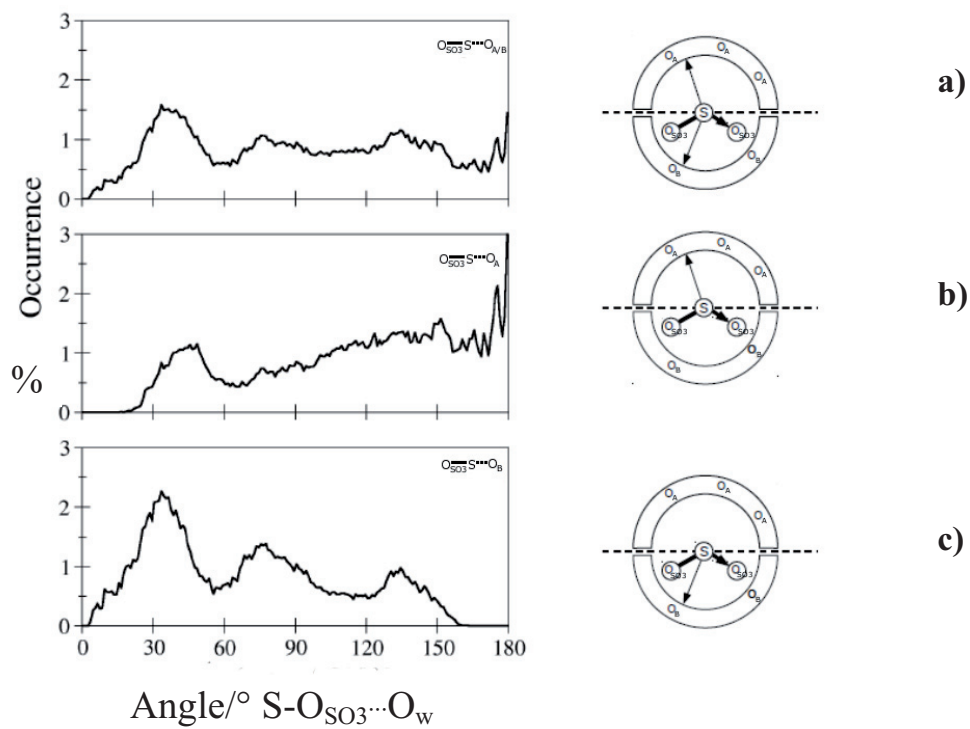


Figure 8

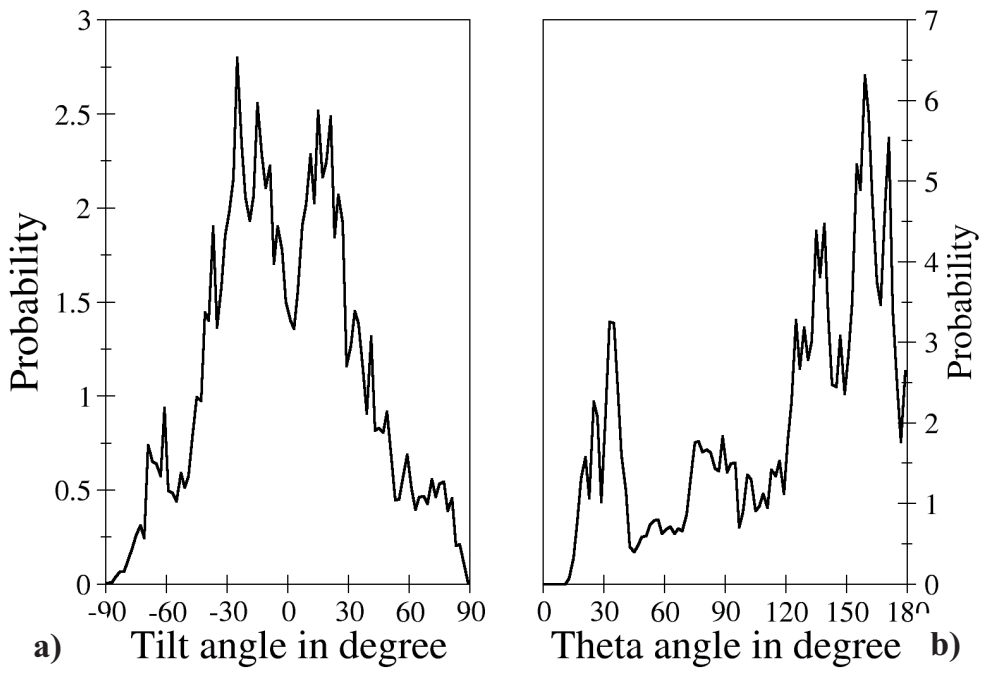
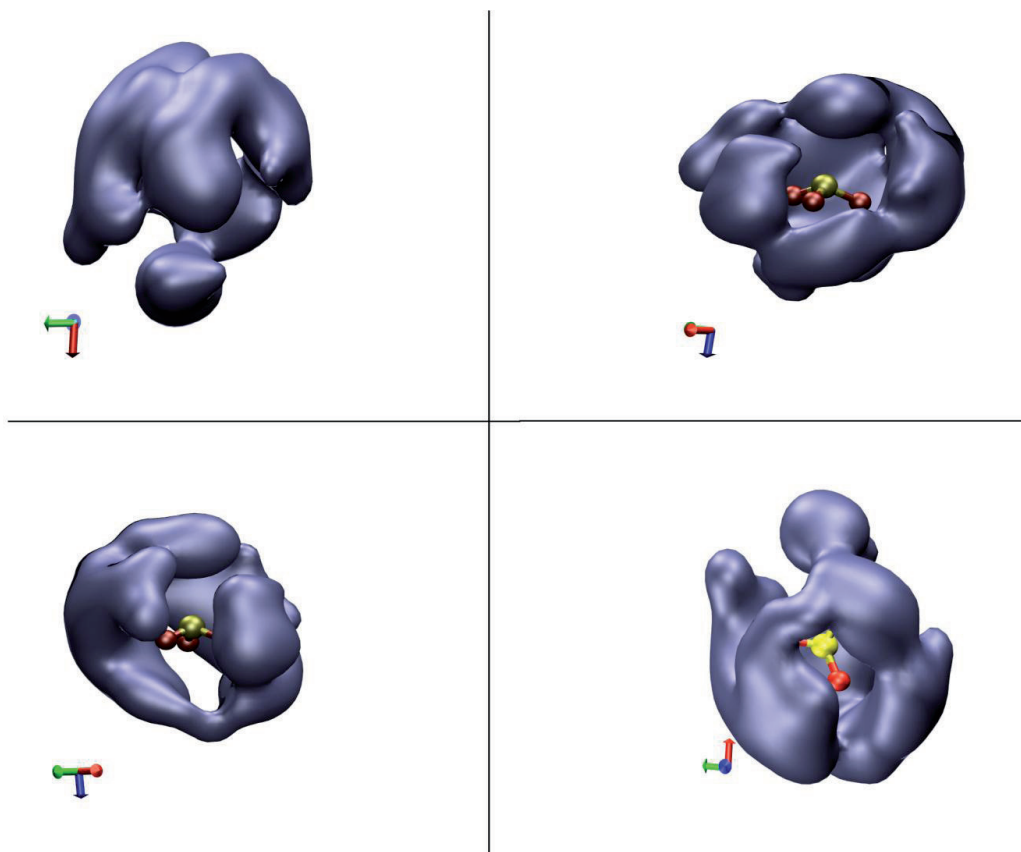
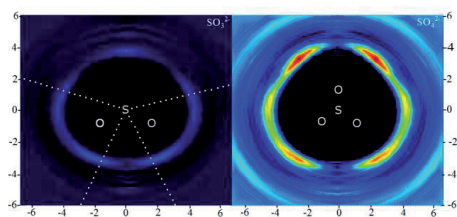


Figure 9



Graphical Abstract



Synopsis

The sulfite ion has an asymmetric hydration sphere with three water molecules are hydrogen bound to each of the sulfite oxygen, and with 3-4 water molecules clustered outside the lone electron-pair. An angular radial distribution analysis has shown that the water exchange takes only place between the water molecules clustered outside the lone electron-pair and the aqueous bulk. This is opposite to the hydrated sulfate ion where the water molecules, symmetrically hydrogen bound to the sulfate oxygens, exchange directly with the aqueous bulk.

**On the Structure and Dynamics of the Hydrated Sulfite Ion in Aqueous Solution
– An ab initio QMCF MD Simulation and Large Angle X-ray Scattering Study**

Lars Eklund,^a Tomas S. Hofer,^b Andreas Pribill,^b Bernd M. Rode^b and Ingmar Persson^{a*}

^a Department of Chemistry, Swedish University of Agricultural Sciences, P.O.Box 7015, SE-750 07 Uppsala, Sweden.

^b Theoretical Chemistry Division, Institute of General, Inorganic and Theoretical Chemistry, University of Innsbruck, Innrain 52a, A-6020 Innsbruck, Austria,

Supporting Material

Complete reference 16

- (16) Frisch, M. J.; Trucks, G. W.; Schlegel, H. B.; Scuseria, G. E.; Robb, M. A.; Cheeseman, J. R.; Montgomery, J.; Vreven, T.; Kudin, K. N.; Burant, J. C.; Millam, J. M.; Iyengar, S. S.; Tomasi, J.; Barone, V.; Mennucci, B.; Cossi, M.; Scalmani, G.; Rega, N.; Petersson, G. A.; Nakatsuji, H.; Hada, M.; Ehara, M.; Toyota, K.; Fukuda, R.; Hasegawa, J.; Ishida, M.; Nakajima, T.; Honda, Y.; Kitao, O.; Nakai, H.; Klene, M.; Li, X.; Knox, J. E.; Hratchian, H. P.; Cross, J. B.; Bakken, V.; Adamo, C.; Jaramillo, J.; Gomperts, R.; Stratmann, R. E.; Yazyev, O.; Austin, A. J.; Cammi, R.; Pomelli, C.; Ochterski, J. W.; Ayala, P. Y.; Morokuma, K.; Voth, G. A.; Salvador, P.; Dannenberg, J. J.; Zakrzewski, V. G.; Dapprich, S.; Daniels, A. D.; Strain, M. C.; Farkas, O.; Malick, D. K.; Rabuck, A. D.; Raghavachari, K.; Foresman, J. B.; Ortiz, J. V.; Cui, Q.; Baboul, A. G.; Clifford, S.; Cioslowski, J.; Stefanov, B. B.; Liu, G.; Liashenko, A.; Piskorz, P.; Komaromi, I.; Martin, R. L.; Fox, D. J.; Keith, T.; Al-Laham, M. A.; Peng, C. Y.; Nanayakkara, A.; Challacombe, M.; Gill, P. M. W.; Johnson, B.; Chen, W.; Wong, M. W.; Gonzalez, C.; Pople, J. A. *Gaussian 03, Revision E.01*.

Table S1. Summary of solid state structures containing individual sulfite ions where the counter ion is monovalent or has a complete hydration shell.*Compounds with isolated sulfite ions*

ICSD code	d(S-O)	Reference
4432	1.505 Å	Larsson, L. O.; Kierkegaard, P. <i>Acta Chem. Scand.</i> 1969 , <i>23</i> , 2253-2260; <i>Powder Diffraction</i> 1986 , <i>1</i> , 265-275. Na ₂ SO ₃ .
1626	1.508 Å	Oddon, Y.; Pepe, G.; Tranquard, A. <i>J. Chem. Res. S</i> 1977 , <i>1977</i> , 138-139. NaTi ₃ (SO ₃) ₂ .
60762	1.515 Å	Andersen, L.; Strömberg, D. <i>Acta Chem. Scand., Ser. A</i> 1986 , <i>40</i> , 479-480. K ₂ SO ₃
23824	1.524 Å	Battelle, L. F.; Trueblood, K. N. <i>Acta Crystallogr.</i> 1965 , <i>19</i> , 531-535. (NH ₄) ₂ SO ₃ ·H ₂ O

Mean 1.513 Å/4*Compounds with sulfite ions forming hydrogen bonds to neighboring hydrated metal ions*

ICSD code	d(S-O)	d(S··H)	Reference
48112	1.528 Å	2.800 Å	Andersen, L.; Lindqvist, O. <i>Acta Crystallogr., Sect. B</i> 1984 , <i>40</i> , 584-586. [Mg(H ₂ O) ₆]SO ₃ .
26149	1.532 Å	2.789 Å	Baggio, S.; Becka, L. N. <i>Acta Crystallogr., Sect. B</i> 1969 , <i>25</i> , 1150-1155. . [Ni(H ₂ O) ₆]SO ₃ .
62636	1.533 Å	2.782 Å	Bats, J. W.; Fuess, H.; Elerman, Y. <i>Acta Crystallogr., Sect. B</i> 1986 , <i>42</i> , 552-557. [Mg(H ₂ O) ₆]SO ₃ .
2524	1.536 Å		Flack, H. D. <i>Acta Crystallogr., Sect. B</i> 1973 , <i>29</i> , 656-658. [Mg(H ₂ O) ₆]SO ₃ .
62637	1.536 Å		Bats, J. W.; Fuess, H.; Elerman, Y. <i>Acta Crystallogr., Sect. B</i> 1986 , <i>42</i> , 552-557. [Mg(H ₂ O) ₆]SO ₃ .
62638	1.536 Å		Bats, J. W.; Fuess, H.; Elerman, Y. <i>Acta Crystallogr., Sect. B</i> 1986 , <i>42</i> , 552-557. [Mg(H ₂ O) ₆]SO ₃ .

Mean 1.534 Å/6

Table S2. Numeric values of the peaks in Figure 2.

Figure 2a

Center	FWHM
1.0	0.058
1.5	0.074
1.9	0.427
2.8	0.324
3.1	0.346
3.7	0.823
4.3	2.011

Figure 2b

Center	FWHM
2.792	0.372
2.994	0.620
4.196	1.435

Figure 2c

Center	FWHM
0.975	0.058
1.921	0.418

Figure 2d

Center	FWHM
1.526	0.075
3.725	0.530
4.114	0.370

Figure 2e

Center	FWHM
2.827	0.330
4.368	2.047



II

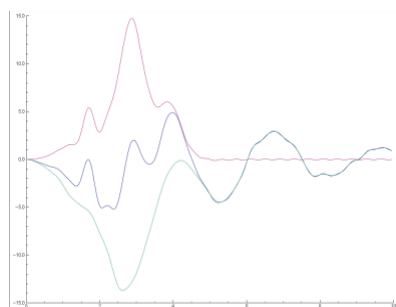


A Comparative Structural Study of Sodium Selenite and Selenate Using Large Angle X-ray Scattering and Double Difference Infrared Spectroscopy

Lars Eklund and Ingmar Persson

Department of Chemistry, Swedish University of Agricultural Sciences, P.O.Box 7015, SE-750 07 Uppsala, Sweden.

Graphical Abstract



Synopsis

The structures of the hydrated selenite and selenate ions have been studied in aqueous solution by LAXS and DDIR. The Se-O bond distances are 1.709(2) and 1.657(2) Å, respectively, which are slightly longer than the mean distances found in the solid state. Each of the selenite and selenate oxygens hydrogen binds on average 2.5 and two water molecules, respectively, which is a lower number than observed for the sulfite and sulfate ions, three. In addition, ca. three water molecules are clustered outside the lone electron-pair on selenium at long distance, 4.3 Å, as also found for the sulfite ion, showing asymmetric hydration for the selenite ion.

Abstract

The structures of the hydrated selenite and selenate ions have been studied in aqueous solution by large angle X-ray scattering, LAXS, and double difference infrared (DDIR) spectroscopy. The Se-O bond distances are 1.709(2) and 1.657(2) Å, respectively, which are slightly longer than the mean distances found in the solid state. The distances found for the first hydration shell of hydrated selenite ion were 3.87(2) Å for Se···O_w, and 4.36(4) Å for the waters clustered outside the selenium lone electron-pair. The selenate ion has a symmetric hydration shell with only one distance, Se···O_w, 3.94(2) Å. The O···O distances for the selenite and selenate oxygens to water oxygens, O···O_w, were not distinguishable from the O_w···O_w distance in the aqueous bulk, giving mean values of 2.873(4) and 2.861(4) Å, respectively. Assuming a mean O_w···O_w distance in the aqueous bulk of 2.89 Å, an estimated O···O_w distance of 2.83-2.86 and 2.81-2.85 Å for the selenite and selenate ions is obtained, respectively. The mean Se-O···O_w angle is 114.5 and 120 ° for the selenite and selenate ions, respectively. The double difference infrared (DDIR) spectra show peaks for affected water bound to the selenite and selenate ions at 2491±2 cm⁻¹ and 2480±39 cm⁻¹, respectively. As these are observed below the peak of bulk water, 2509 cm⁻¹, the selenite and selenite ions are both regarded as weak structure makers.

Introduction

The selenium oxo acids and their salts have many similarities with the corresponding sulfur oxo acids, including similar physico-chemical parameters.¹ The structure and hydrogen bonding of the hydrated sulfite and sulfate ions has been studied previously.²⁻⁴ Three water molecules are hydrogen bound to each oxygen atom in both ions. Furthermore, some water molecules are clustered outside the lone electron-pair of the sulfite ion at a fairly well-defined distance. The sulfite and sulfate ions are both weak structure makers, thus the hydrogen bond between the sulfite/sulfate oxygens and the hydrating water molecules is slightly shorter and stronger than between water molecules in the aqueous bulk. It is of fundamental interest to compare the hydration of the corresponding selenium oxo anions with the sulfur ones from both structural and hydrogen bond strength point of view. An overview of the structures of the selenous acid-hydrogenselenite ion-selenite ion and the selenic acid-hydrogenselenate ion-selenate ion system will be presented and analyzed.

Experimental

Chemicals. *Sodium selenate*, Na₂SeO₄ (analytical grade, Fluka), *sodium selenite*, Na₂SeO₃ (analytical grade, Fluka) and *heavy water*, D₂O, (99.96 atom % D, Aldrich) were used without further purification.

Solutions. The solutions for the LAXS experiments were prepared by dissolving weighed amount of sodium selenite and selenate, respectively, in deionized Milli Q filtered water. The compositions of the studied solutions are given in Table 1.

For IR measurements matched concentration series in both pure water and 4% w/w D₂O/H₂O where prepared for both sodium selenate and sodium selenite.

LAXS. The scattering of MoK α X-ray radiation, $\lambda=0.7107$ Å, from the free surface of the aqueous sodium selenite and selenate solutions were measured in a large angle Θ - Θ goinometer described elsewhere.⁵ The solution was contained in a teflon cup filled until a positive meniscus was observed generating a flat surface in the irradiated region. The container was placed inside an air-tight radiation shield with beryllium windows. The scattered radiation was monochromatised using a LiF (200) single crystal focusing monochromator. The scattering was determined at 446 angles in the angle range of $0.5 < \Theta < 65^\circ$, where the scattering angle is 2Θ . At each angle 100,000 X-ray quanta were accumulated, and the entire angle range was scanned twice corresponding to a statistical error of about 0.3 %. The divergence of the x-rays was defined through combination of divergence-collecting-focal slits of $\frac{1}{4}^\circ$ - $\frac{1}{2}^\circ$ - 0.2° .

mm and 1° - 2° - 0.2 mm. Three different Θ -regions were scanned to get a suitable counting rate and change in angle, with overlapping regions to enable scaling of the data. The data collection and treatment is described in detail elsewhere.⁵ All data treatment was carried out using the KURVLR program,⁶ and the structural parameters in the theoretical model were refined by minimizing $U = w(s)\Sigma s^2[i_{\text{exp}}(s)-i_{\text{calc}}(s)]^2$ using the STEPLR program.^{7,8} The experimental data was normalized to a stoichiometric unit containing one selenium atom, using the scattering factors f for neutral atoms, including corrections for anomalous dispersion, $\Delta f'$ and $\Delta f''$,⁹ Compton scattering^{10,11} and multiple scattering events.

Double differential FTIR. The IR measurements were performed in a continuous series on a Perkin-Elmer Spectrum 100 FT-IR Spectrophotometer with matched concentrations of the two solutions in a temperature controlled liquid cell using 3mm CaF₂ windows (PIKE Technologies), the cell was heated to $25^{\circ}\text{C} \pm 0.5^{\circ}\text{C}$.

Each spectrum was measured for 256 scans with 4 cm^{-1} resolution in the range $4000\text{-}900\text{ cm}^{-1}$. The path length was 0.035280 mm determined through interference.¹² By measuring the same concentration of salt in both H₂O and HDO solution and then subtracting pure solutions without solute one gets an infrared spectrum of the HDO molecules different from those in the aqueous bulk. By taking the derivative of these spectra $\partial\epsilon/\partial m$ where ϵ is the spectra and m the molality of the solution then subtracting $(1/N*M)*\partial\epsilon/\partial m$ from the spectrum of pure water, where N is the affected number of water and M is the mean molar mass in kg/mol of water and partially heavy water, as described by Kristiansson et al. and in Gampe et al.,^{13,14,15} the affected water peaks ascribed to water molecules bound to cations or anions can be found through PCA. All calculations of the spectra was carried out using GRAMS AI version 8.0 (Thermo-Fisher Scientific) and RAZOR tools(Spectrum Square Associates), and the Array Basic program YANUZ.AB¹⁶ was used to calculate derivatives of spectra.

Results and Discussion

Large angle X-ray scattering

The experimental radial distribution function (RDF) of the aqueous solution of sodium selenate shows three peaks at $1.657(4)$, $2.861(8)$ and $3.94(4)\text{ \AA}$, after refinement, corresponding the Se-O bond distance in the hydrated selenate ion, the O \cdots O distances in the aqueous bulk and between selenate oxygens and hydrating water molecules, and Se \cdots O distances between selenium atom and the hydrating water molecules, respectively, Figure 1.

The hydrated sodium ion is observed as a weak shoulder at 2.43(4) Å, after refinement, Figure 1, is in complete agreement with previous studies.¹⁷ The observed Se-O bond distance in aqueous solution is slightly longer, 0.023 Å than the mean Se-O bond distance in solid selenate salts, Table S1. This is within the expected range as the hydration through the hydrogen bonding electrostatically interact with the selenate oxygens. The increase in the Se-O bond length is the same order as previously observed for the sulfate and perchlorate ions.^{2,18} The distance between the central Se atom the oxygens of the hydrating water molecules, Se···O_{aq}, 3.94 Å, shows that the \angle Se-O-O_{aq} angle of 120 ° assuming an O···O_{aq} distance of 2.83 Å (see below). As the water molecules hydrating the selenate oxygens are electrostatic the \angle Se-O-O_{aq} angle of 120 ° strongly indicates that on average two water molecules are hydrogen bound to each selenate oxygen. This is in contradiction to the sulfate and perchlorate ions where three water molecules are hydrogen bound to each sulfate and perchlorate oxygen. The O···O distances in the aqueous bulk and between selenate oxygens and hydrating water molecules are not possible to separate, and a mean O···O distance of 2.861(8) Å was obtained. This mean O···O distance is slightly shorter than normally observed for the aqueous bulk, 2.89 Å. This strongly indicates that the O···O_{aq} distance is in the range 2.81-2.85 Å, showing that the selenate ion is a structure maker as also shown in the DDIR measurements, see below.

The RDF of the aqueous solution of sodium selenite shows three peaks at 1.709(4), 2.873(8) and 3.87(4) Å, after refinement, corresponding the Se-O bond distance in the hydrated selenite ion, the O_{aq}···O_{aq} and O···O_{aq} distances, and Se···O distances between selenium atom the hydrating water molecules, respectively, Figure 2. The latter peak is unusually broad strongly indicating an additional Se···O distance at 4.36(8) Å, as also found in the hydrated sulfite ion.⁴ Assuming an O···O_{aq} distance of 2.85 Å, see below, the \angle Se-O-O_{aq} angle becomes 114 °, thus between the expected values of 109.47 and 120.0 for tetrahedral and trigonal configuration around the selenite oxygens. Furthermore, the temperature coefficient is very large, twice the value observed for the selenate ion, Table 2, which shows a very broad distance distribution. It seems therefore likely that the selenite oxygen hydrogen bind to two or three water molecules, and that the observed Se···O_{aq} distance and the large temperature coefficient are average values. The additional Se···O_{aq} distance at 4.36(8) Å does most probably belong to the water molecules clustered outside the lone electron-pair on the selenium.

The mean value of the O···O distance in the aqueous bulk and between selenate oxygens

and hydrating is slightly shorter, 2.873(4) Å, than in the aqueous bulk, 2.89 Å. The observed mean O···O distance indicate that the O···O_{aq} distance is in the range 2.83-2.86 Å, showing that the selenate ion is a structure maker but as such weaker than the selenite ion as also shown in the DDIR measurements, see below.

Fourier transform infrared spectroscopy

Analysis of the affected spectra of selenite, Figure 3, through spectral decomposition generates number of affected waters as $N=15.7$ and a sodium peak at $2534\pm 9\text{ cm}^{-1}$ in good agreement with earlier work.^{15,19,20,21,22,23} The main anionic peak of the hydrated selenite ion is at $2491\pm 2\text{ cm}^{-1}$. The position of the anionic peak indicates that selenite ion is a weak structure maker with molecular interaction energy of water $\Delta U_w = -45.2\text{ kJ mol}^{-1}$ derived from ν_{OD} using the Badger-Bauer rule²⁴ and the calculations detailed in earlier work^{14,15}

The selenate affected DDIR spectra are given in Figure 4, and it was possible to separate the contributions from the sodium and selenate ions. The peak ascribed to the selenate ion has a maximum at $2480\pm 39\text{ cm}^{-1}$. Transforming the ν_{OD} for the affected water peak to molecular interaction energy of water $\Delta U_w = -47.4\text{ kJ}\cdot\text{mol}^{-1}$ calculated as above. The peak ascribed to the sodium ion is observed at $2539\pm 18\text{ cm}^{-1}$. The peak is a slightly wider peak than earlier work, but the peak position is within expected range.

Structure of selenate and selenite ions in solid state and aqueous solution

The Se-O bond distances in available data bases for the selenous acid-hydrogenselenite ion-selenite ion and the selenic acid-hydrogenselenate ion-selenate ion systems are summarized in Table S1. The selenite and selenate ions have regular truncated tetrahedral and tetrahedral structure, respectively, with all Se-O bond distances the same or almost the same, mean 1.691 and 1.634 Å, Table S1. As shown above, the Se-O bond distances increase by about 0.02 Å at hydration in aqueous solution. The structures of selenous acid, hydrogenselenite ion, selenic acid and hydrogenselenate ion display a different pattern with the Se-O bonds where the oxygen is protonated significantly longer than oxygens without any proton. The difference in mean Se-O bond distance in these two kinds of oxygens in the hydrogenselenite and hydrogenselenate ions is 0.107 and 0.090 Å, respectively, and about the same differences are found for the selenous and selenic acid, 0.118 and 0.089 Å, respectively. This difference is expected to be maintained also in aqueous solution as the difference in hydrogen bond strength when the selenite/selenate oxygen is a hydrogen bond acceptor or the OH group as a hydrogen bond donor is expected to be small. It is not possible to distinguish such small differences with the

structural methods applicable on aqueous solution available today. However, the mean Se-O bond distance for the hydrogenselenite ion, selenous acid, hydrogenselenate ion and selenic acid is very close to the mean Se-O bond distance in the selenite and selenate ions with 1.691, 1.699 and 1.700 Å for SeO_3^{2-} , HSeO_3^- and H_2SeO_3 , respectively, and 1.634, 1.638 and 1.642 Å for SeO_4^{2-} , HSeO_4^- and H_2SeO_4 , respectively, Table S1.

Conclusions

The structures of the hydrated selenite and selenate ions in aqueous solution show a single shell of water molecules hydrogen bound to the oxygen atoms. In addition, outside the lone electron-pair of the selenite ion about three water molecules are clustered at long distance. To the oxygens of the hydrated selenite and selenate ions on average ca. 7.5 and eight water molecules are coordinated, respectively. These numbers are lower than for the corresponding sulfuroxo-anions where three water molecules are hydrogen bound to each of the oxygen. Additionally around the selenium lone-pair of selenite three water molecules are clustered at a longer distance. Selenite and selenate ions are both weak structure makers as shown by O-D stretching frequencies of the hydrating water molecules in comparison with the value in pure water. The symmetric and more oxidized selenate is a stronger structure maker than selenite but a weaker than the sulfate and fluoride anions^{4, 23}. For more information on the influence of asymmetric hydration mechanism of the selenite ion on the difference in coordination further studies using computer simulations would be needed.

Acknowledgment

The financial support from the Swedish Research Council is gratefully acknowledged.

References

1. Greenwood, N. N.; Earnshaw, A. *The Chemistry of the Elements*, 2nd Ed., Elsevier, Oxford, Chap. 16.2.6.
2. Vchirawongkwin, V.; Rode, B. M.; Persson, I. *J. Phys. Chem. B* **2007**, *111*, 4150-4155.
3. Bergström, P.-Å.; Lindgren, J.; Kristiansson, O. *J. Phys. Chem.* **1991**, *95*, 8575-8580.
4. Eklund, L. ; Hofer, T. S. ; Pribil, A. ; Rode, B. M. ; Persson, I., submitted for publication to *Inorg. Chem.*
5. Stålhandske, C. M. V.; Persson, I.; Sandström, M.; Kamienska-Piotrowicz, E. *Inorg. Chem.* **1997**, *36*, 3174-3182.
6. Johansson, G.; Sandström, M. *Chem. Scr.* **1973**, *4*, 195.
7. Molund, M.; Persson, I. *Chem. Scr.* **1985**, *25*, 197.
8. Chandler, J. P. *Behav. Sci.* **1969**, *14*, 81-82.
9. Wilson, Ed. *International Tables for Crystallography*; Kluwer Academic Publishers: Dordrecht, The Netherlands, 1995; Vol. C.
10. Cromer, D. T. *J. Chem. Phys.* **1967**, *47*, 1892-1894.
11. Cromer, D. T. *J. Chem. Phys.* **1969**, *50*, 4857-4859.
12. Pike Technologies application note -0501.
13. Kristiansson, O.; Lindgren, J.; De Villepin, J. *J. Phys. Chem.* **1988**, *92*, 2680-2685
14. Stangret, J.; Gampe, T. *J. Phys. Chem.* **1999**, *103*, 3778-3783.
15. Stangret, J.; Gampe, T. *J. Phys. Chem. A* **2002**, *106*, 5393-5402.
16. Array Basic program YANUZ.AB provided by M. Smiechowski, Technical University of Gdansk, Poland
17. Mähler, J.; Persson, I., submitted to *J. Am. Chem. Soc.*
18. Persson, I.; Lyczko, K.; Lundberg, D.; Eriksson, L.; Placzek, A. *Inorg. Chem.* **2011**, *50*, 1058-1072.
19. Eriksson, A.; Kristiansson, O.; Lindgren, J. *J. Mol. Struct.* **1984**, *114*, 455.
20. Stangret, J.; Kamienska-Piotrowicz, E. *J. Chem. Soc., Faraday Trans.* 1997, *93*, 3463.
21. Lindgren, J.; Kristiansson, O.; Paluszkiwicz, C. *Interactions of Water in Ionic and Nonionic Hydrates*; Kleeberg, H., Ed.; Springer-Verlag: Berlin, Heidelberg, 1987; p 43.
22. Kristiansson, O.; Eriksson, A.; Lindgren, J. *Acta Chem. Scand.* 1984, *A38*, 613
23. Kristiansson, O.; Lindgren, J. *J. Mol. Struct.*, 1988, *177*, 537.
24. Badger, R. M.; Bauer, S. H. *J. Chem. Phys.* **1937**, *5*, 839-851.

Table 1. Concentrations ($\text{mol}\cdot\text{dm}^{-3}$) of the aqueous sodium selenite and selenate solutions used in the LAXS measurements.

Sample	$[\text{SeO}_x^{2-}]$	$[\text{Na}^+]$	[water]	$\rho/\text{g}\cdot\text{cm}^{-3}$	μ/cm^{-1}
Na_2SeO_3 in water	1.5006	3.0012	49.2073	1.170	10.27
Na_2SeO_4 in water	1.5066	3.0132	50.2768	1.1904	10.33

Table 2. Mean bond distances, $d/\text{\AA}$, number of distances, N , and temperature coefficients, $b/\text{\AA}^2$, the half-height full width, $l/\text{\AA}$, in the LAXS study of aqueous sodium selenite and selenate solutions at room temperature.

Species	Interaction	N	d	b	l
<i>1.5066 mol·dm⁻³ Na₂SeO₄ in water</i>					
$[\text{SeO}_4(\text{H}_2\text{O})_{12}]^{2-}$	Se-O	4	1.657(2)	0.0022(3)	0.21
	Se···O _{II}	8	3.94(2)	0.028(2)	0.24
$\text{Na}(\text{H}_2\text{O})_6^+$	Na-O	6	2.43(2)	0.022(2)	0.21
Aqueous bulk	O···O	2	2.861(4)	0.018(4)	0.19
<i>1.5006 mol·dm⁻³ Na₂SeO₃ in water</i>					
$[\text{SeO}_3(\text{H}_2\text{O})_9(\text{H}_2\text{O})_{-3}]^{2-}$	Se-O	3	1.709(2)	0.0031(3)	0.079
	Se···O _{II}	7.5	3.87(2)	0.050(2)	0.33
	Se···O _{II}	~3	4.36(4)	0.027(2)	0.23
$\text{Na}(\text{H}_2\text{O})_6^+$	Na-O	6	2.42(2)	0.023(2)	0.21
Aqueous bulk	O···O	2	2.873(4)	0.025(1)	0.22

Table 3. O-D stretching frequencies of the water molecules hydrating the selenate, sulfate, selenite and sulfite ions.

Ion	$\nu(\text{O-D})/\text{cm}^{-1}$	Ref.
$[\text{SeO}_3(\text{H}_2\text{O})_9(\text{H}_2\text{O})_{-3}]^{2-}$	<i>TBD</i>	^a
$[\text{SeO}_3(\text{H}_2\text{O})_{7.5}(\text{H}_2\text{O})_{-3}]^{2-}$	2491	^a
$[\text{SO}_4(\text{H}_2\text{O})_{12}]^{2-}$	2477	3
$[\text{SeO}_4(\text{H}_2\text{O})_8]^{2-}$	2480	^a

^a This work.

Legends to Figures

Figure 1 LAXS. $\text{SeO}_4^{2-}(\text{aq})$ (a) Individual peak shapes for all theoretical contributing species in the $1.5006 \text{ mol}\cdot\text{dm}^{-3}$ aqueous solution of hydrated selenate. The hydrated selenate ion (blue line), hydrated sodium ion (purple line) and the aqueous bulk (green line). (b) Experimental $D(r) - 4I/r^2\rho_0$ (blue line); model (purple line), the modelled distances are given in table 1; difference (green line). (c) Reduced LAXS intensity function, $si(s)$ (blue line); model $si_{\text{calc}}(s)$ (purple line).

Figure 2 LAXS $\text{SeO}_3^{2-}(\text{aq})$. (a) Individual peak shapes for all theoretical contributing species in the $1.5006 \text{ mol}\cdot\text{dm}^{-3}$ aqueous solution of hydrated selenite, the hydrated selenite ion (blue line), hydrated sodium ion (black line) and the aqueous bulk (red line). (b) Experimental $D(r) - 4I/r^2\rho_0$ (blue line); model (red line), the modelled distances are given in table 1; difference (green line). (c) Reduced LAXS intensity function, $si(s)$ (blue line); model $si_{\text{calc}}(s)$ (purple line).

Figure 3 Double differential FTIR $\text{SeO}_3^{2-}(\text{aq})$. By PCA analysis using gaussian peak shapes of the affected spectra. The analytical peaks could be found at the affected spectra (black) where $N=15.7$, the anionic peaks yellow and green at 2408 ± 6 and 2491 ± 2 , where yellow represents the asymmetric contributions. The sodium peak is represented by represents the red main peak at 2534 ± 9 and peak number blue at 2656 ± 2 which is well in agreement with earlier work. The tail at lower wavenumbers than 2300 is not associated with the O-D stretch of affected water.

Figure 4 Double differential FTIR $\text{SeO}_4^{2-}(\text{aq})$. By PCA analysis using gaussian peak shapes of the affected spectra. The analytical peaks could be found at the affected spectra (black) where $N=12.9$, the anionic peaks green, purple and yellow, where purple and yellow represents the asymmetric contributions. For the sodium peak red represents the main peak which is well in agreement with erlier work and the blue is a asymmetric peak cointribution.

Figure 1

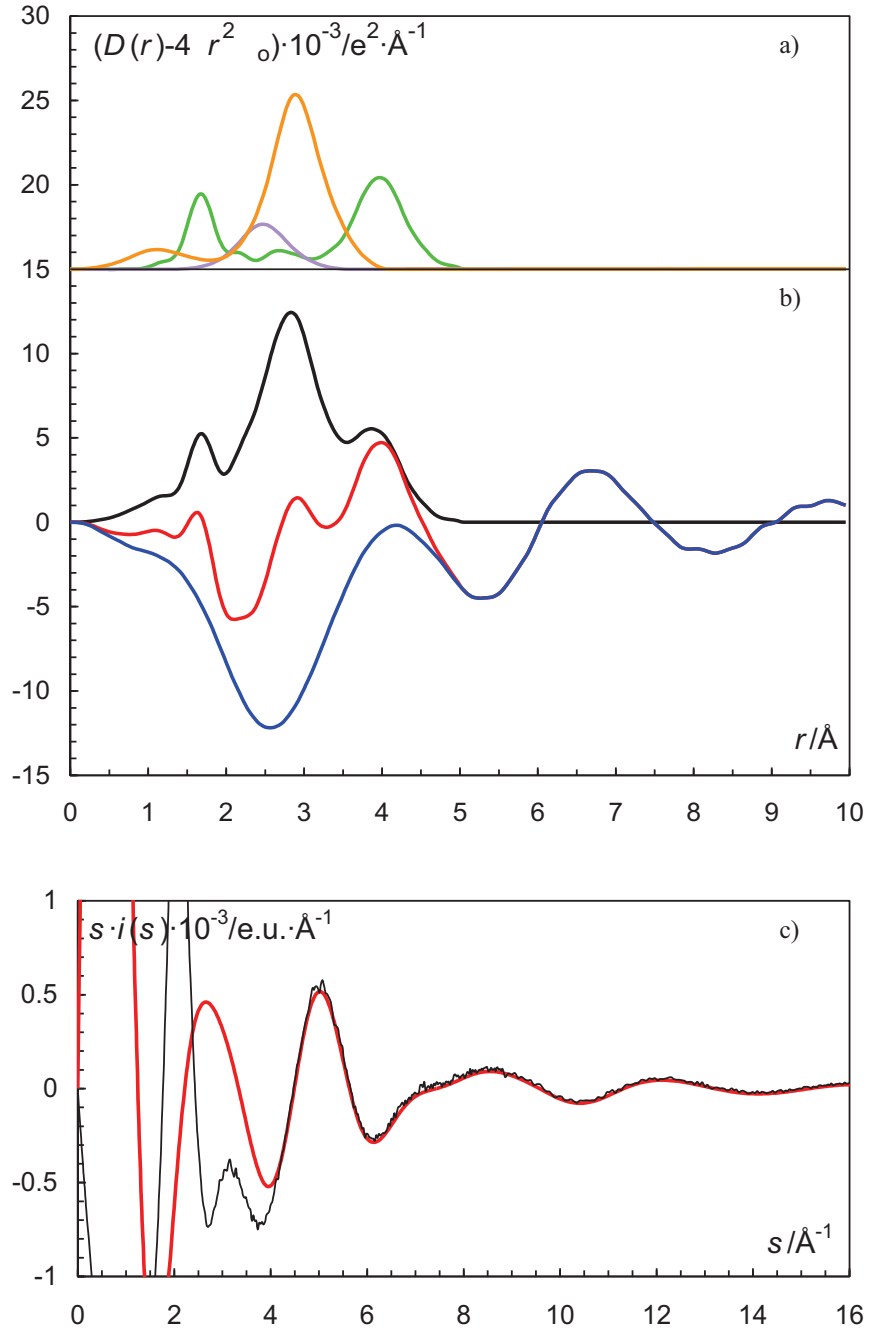


Figure 2

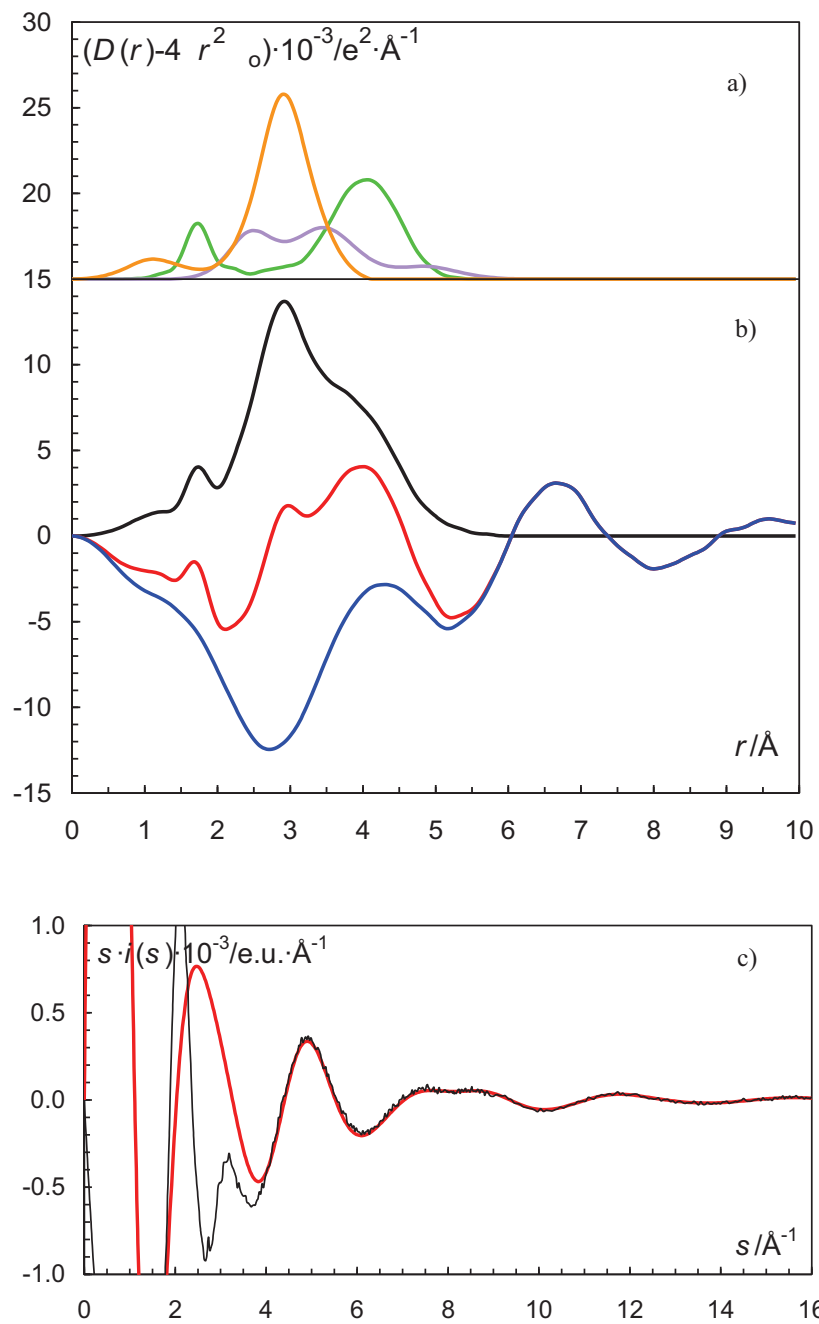


Figure 3

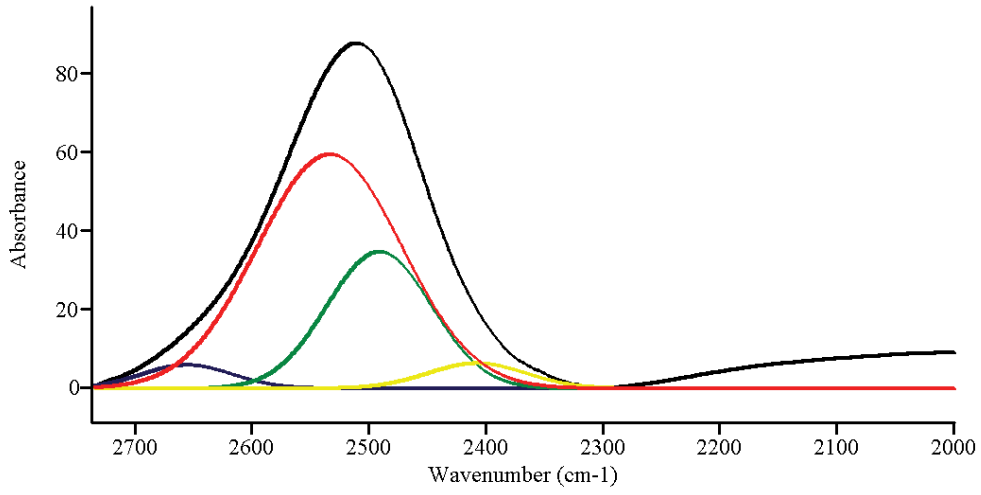


Figure 4

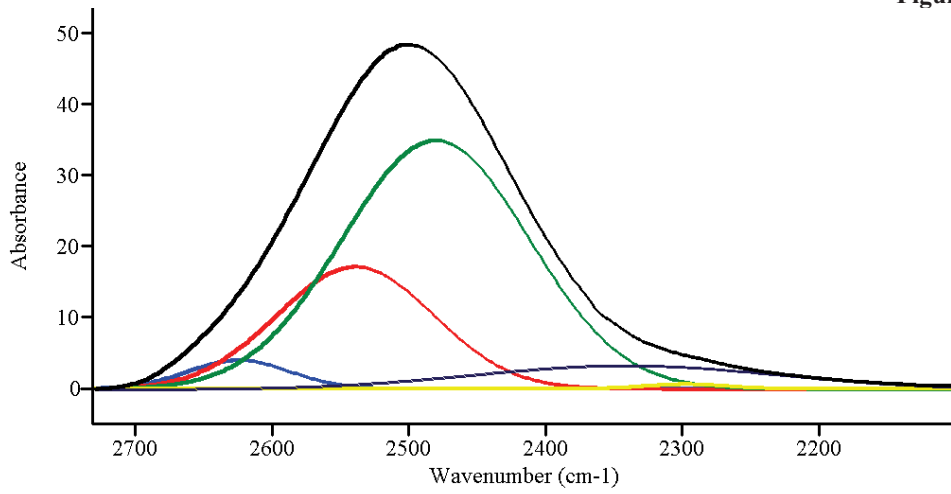


Table S1. Summary of Se-O bond distances solid state structures of selenate ion, hydrogenselenate ion, selenic acid, selenite ion, hydrogenselenite and selenous acid from the Inorganic Crystal Structure Database (ICSD) and Cambridge Structure Database (CSD). References in red are not included in the average value.

Selenate ion, SeO₄²⁻		
ICSD/ CSD code	d(Se-O)/Å	Reference Formula of compound
73411	1.600 Å	Fabry, J.; Brezewski, T. <i>Acta Crystallogr., Sect. C</i> 1993 , <i>49</i> , 1724-1727. Tl ₂ SeO ₄
419775	1.617 Å	Grzechnik, A.; Brezewski, T.; Friese, K. <i>J. Solid State Chem.</i> 2008 , <i>181</i> , 2914-2917. Tl ₂ SeO ₄
99382	1.618 Å	Friese, K.; Goeta, A. E.; Leech, M. A.; Howard, J. A. K.; Madariaga, G.; Perez-Mato, J. M.; Brezewski, T. <i>J. Solid State Chem.</i> 2004 , <i>177</i> , 1127-1136. Tl ₂ SeO ₄
21047	1.620 Å	Kruglik, A. I.; Simonov, V. I.; Yuzvak, V. I. <i>Kristallografiya</i> 1973 , <i>18N</i> , 287-292. (NH ₄)NaSeO ₄ ·2H ₂ O
157371	1.620 Å	Dammak, M.; Litaïem, H.; Graveriau, P.; Mhiri, T.; Kolsi, A. W. <i>J. Alloys Compd.</i> 2007 , <i>442</i> , 316-319. Rb ₂ SeO ₄ ·Te(OH) ₆
419338	1.621 Å	Ghedia, S.; Dinnebier, R.; Jansen, M. <i>Solid State Sci.</i> 2009 , <i>11</i> , 72-76. Rb ₂ SeO ₄
14298	1.622 Å	Kalman, A.; Stephens, J. S.; Cruickshank, D. W. <i>J. Acta Crystallogr., Sect. B</i> 1970 , <i>26</i> , 1451-1454. K ₂ SeO ₄
107620	1.622 Å	Malchus, M.; Jansen, M. <i>Z. Naturforsch., Teil B</i> 1998 , <i>53</i> , 704-710. (N(CH ₃) ₄) ₂ SeO ₄
200539	1.622 Å	Nozik, Y. Z.; Fykin, L. E.; Duderov, V. Y.; Muradyan, L. A.; Rostuntseva, A. I. <i>Kristallografiya</i> 1978 , <i>23N</i> , 617-619. Na(NH ₄)SeO ₄ ·2H ₂ O
73464	1.624 Å	Fabry, J.; Brezewski, T.; Petricek, V. <i>Acta Crystallogr., Sect. B</i> 1993 , <i>49</i> , 826-832. K ₃ Na(SeO ₄) ₂
81688	1.624 Å	Gonzalez-Silgo, C.; Solans, X.; Ruiz-Perez, C.; Martinez-Sarrion, M. L.; Mestres, L. <i>Ferroelectrics</i> 1996 , <i>177</i> , 191-199. K ₂ SeO ₄
99383	1.625 Å	Friese, K.; Goeta, A. E.; Leech, M. A.; Howard, J. A. K.; Madariaga, G.; Perez-Mato, J. M.;

81689	1.626 Å	Breczewski, T. <i>J. Solid State Chem.</i> 2004 , <i>177</i> , 1127-1136. Tl_2SeO_4
81690	1.626 Å	Gonzalez-Silgo, C.; Solans, X.; Ruiz-Perez, C.; Martinez-Sarrion, M. L.; Mestres, L. <i>Ferroelectrics</i> 1996 , <i>177</i> , 191-199. K_2SeO_4
54168	1.627 Å	Gonzalez-Silgo, C.; Solans, X.; Ruiz-Perez, C.; Martinez-Sarrion, M. L.; Mestres, L. <i>Ferroelectrics</i> 1996 , <i>177</i> , 191-199. K_2SeO_4
158790	1.628 Å	Fukami, T.; Chen, R.-H. <i>Acta Phys. Pol., Ser. A</i> 1998 , <i>94</i> , 795-801. $\text{K}_3\text{Na}(\text{SeO}_4)_2$
250316	1.628 Å	Krivovichev, S. V. <i>Ukrain. Dokl. Kristallogr.</i> 2006 , <i>135</i> , 106-113. $[\text{Al}(\text{H}_2\text{O})_6]_2(\text{SeO}_4)_3(\text{NO}_3) \cdot 4\text{H}_2\text{O}$
419776	1.628 Å	Krivovichev, S. V. <i>Zapiski Vserossijskogo Mineralogicheskogo Obshchestva</i> 2006 , <i>135</i> , 106-113. $[\text{Al}(\text{H}_2\text{O})_6]_2(\text{SeO}_4)_3 \cdot 4\text{H}_2\text{O}$
81691	1.630 Å	Grzechnik, A.; Breczewski, T.; Friese, K. <i>J. Solid State Chem.</i> 2008 , <i>181</i> , 2914-2917. Tl_2SeO_4
94517	1.630 Å	Gonzalez-Silgo, C.; Solans, X.; Ruiz-Perez, C.; Martinez-Sarrion, M. L.; Mestres, L. <i>Ferroelectrics</i> 1996 , <i>177</i> , 191-199. K_2SeO_4
160681	1.630 Å	Troyanov, S. I.; Kosterina, E. V.; Kemnitz, E. <i>Zh. Neorg. Khim.</i> 2001 , <i>46</i> , 1496-1502. $\text{Cs}_4(\text{SeO}_4)(\text{HSeO}_4)_2 \cdot \text{HF}$
281276	1.630 Å	Smirnov, L. S.; Melnyk, G.; Zink, N.; Wozniak, K.; Dominiak, P.; Pawlukoje, A.; Loose, A.; Shuvalov, L. A. <i>Poverkhnostnye Fizika, Khimiya, Mekhanika</i> 2007 , <i>73-79</i> . $(\text{NH}_4)_2(\text{SeO}_4)_2$
710013	1.630 Å	Johnston, M. G.; Harrison, W. T. A. <i>Acta Crystallogr., Sect. E</i> 2003 , <i>59</i> , i25-i27. $\text{Li}_2\text{SeO}_4 \cdot \text{H}_2\text{O}$
RUXWIQ	1.630 Å	Euler, H.; Barbier, B.; Meents, A.; Kirfel, A. <i>Z. Kristallogr. - New Crystal Struct.</i> 2009 , <i>224</i> , 360-364. $\text{Tl}_2[\text{Zn}(\text{H}_2\text{O})_6](\text{SeO}_4)_2$
60928	1.631 Å	Nemec, I.; Gyepes, R.; Micka, Z.; Trojanek, F. <i>Mat. Res. Soc. Symp. Proc.</i> 2002 , <i>725</i> , 213. $(\text{C}_5\text{H}_{12}\text{NO}_2)_2\text{SeO}_4 \cdot 2\text{H}_2\text{O}$. K. Marchewka, J. Janczak, S. Debrus, J. Baran, H. Ratajczak
73463	1.631 Å	Takahashi, I.; Onodera, A.; Shiozaki, Y. <i>Acta Crystallogr., Sect. C</i> 1987 , <i>43</i> , 179-182. Rb_2SeO_4
150083	1.631 Å	Fabry, J.; Breczewski, T.; Petricek, V. <i>Acta Crystallogr., Sect. B</i> 1993 , <i>49</i> , 826-832. $\text{K}_3\text{Na}(\text{SeO}_4)_2$
		Wildner, M.; Stoilova, D.; Georgiev, M.; Karadjova, V. <i>J. Mol. Struct.</i> 2004 , <i>707</i> , 123-130. $[\text{Be}(\text{H}_2\text{O})_4]_2\text{SeO}_4$

710012	1.631 Å	Euler, H.; Barbier, B.; Meents, A.; Kirfel, A. Z. <i>Kristallogr. - New Crystal Struct.</i> 2009 , 224, 360-364. $\text{Ti}_2[\text{Ni}(\text{H}_2\text{O})_6](\text{SeO}_4)_2$
PRACSE10	1.631 Å	Morosin, B.; Howatson, J. <i>Acta Crystallogr., Sect. B</i> 1970 , 26, 2062. $[\text{Cu}(\text{H}_2\text{N}(\text{CH}_2)\text{NH}_2)_2]\text{SeO}_4 \cdot \text{H}_2\text{O}$
27656	1.632 Å	Mehrotra, B. N.; Hahn, T.; Eysel, W.; Roepke, H.; Illguth, A. <i>Neues Jahrbuch fuer Mineralogie. Monatshefte</i> 1978 , 408-421. Na_2SeO_4
61183	1.632 Å	Kruglik, A. I. <i>Dokl. Akad. Nauk SSSR</i> 1976 , 229, 853-855. $\text{Na}(\text{NH}_4)(\text{SeO}_4) \cdot 2\text{H}_2\text{O}$
158480	1.632 Å	Krivovichev, S. V. <i>Ukrain. Dokl. Kristallogr.</i> 2006 , 135, 80-87. $[\text{Mg}(\text{H}_2\text{O})_4]_2(\text{SeO}_4)_2 \cdot \text{H}_2\text{O}$
200912	1.632 Å	Mukhtarova, N. N.; Rastsvetaeva, R. K.; Ilyukhin, V. V.; Belov, N. V. <i>Kristallografiya</i> 1979 , 24N, 1184-1192. $\text{Na}[\text{In}(\text{H}_2\text{O})_6](\text{SeO}_4)_2$
250370	1.632 Å	Krivovichev, S. V. <i>Zapiski Vserossijskogo Mineralogicheskogo Obshchestva</i> 2006 , 80-87. $[\text{Mg}(\text{H}_2\text{O})_4]_2(\text{SeO}_4)_2 \cdot \text{H}_2\text{O}$
710008	1.632 Å	Euler, H.; Barbier, B.; Meents, A.; Kirfel, A. Z. <i>Kristallogr. - New Crystal Struct.</i> 2009 , 224, 360-364. $\text{Ti}_2[\text{Mg}(\text{H}_2\text{O})_6](\text{SeO}_4)_2$
RANYEK	1.632 Å	Havlicek, D.; Plocek, J.; Nemeec, I.; Gyepes, R.; Micka, Z. <i>J. Solid State Chem.</i> 2000 , 150, 305. $(\text{C}_6\text{H}_{16}\text{N}_2)\text{SeO}_4 \cdot 2\text{H}_2\text{O}$
WUYXIX	1.632 Å	Marchewka, M. K.; Janczak, J.; Debrus, S.; Baran, J.; Ratajczak, H. <i>Solid State Sci.</i> 2003 , 5, 643. $(\text{C}_3\text{H}_7\text{N}_{0.4})(\text{SeO}_4)_2 \cdot 3\text{H}_2\text{O}$
82757	1.633 Å	Micka, Z.; Prokopova, L.; Cisarova, I.; Havlicek, D. <i>Coll. Czech. Chem. Commun.</i> 1996 , 61, 1295-1306. $\text{Rb}_2[\text{Mg}(\text{H}_2\text{O})_6](\text{SeO}_4)_2$
174115	1.633 Å	Sawae, S.; Nakashima, T.; Shigematsu, H.; Kasano, H.; Mashiyama, H. <i>J. Phys. Soc. Jpn.</i> 2005 , 74, 2748-2753. $(\text{K}_{0.52}\text{Rb}_{0.48})_2\text{SeO}_4$
240671	1.633 Å	Ling, J.; Albrecht-Schmitt, T. E. <i>Inorg. Chem.</i> 2007 , 46, 346-347. $\text{K}_2\text{SeO}_4 \cdot 2\text{HIO}_3$
710009	1.633 Å	Euler, H.; Barbier, B.; Meents, A.; Kirfel, A. Z. <i>Kristallogr. - New Crystal Struct.</i> 2009 , 224, 360-364. $\text{Ti}_2[\text{Co}(\text{H}_2\text{O})_6](\text{SeO}_4)_2$
RANYAG	1.633 Å	Havlicek, D.; Plocek, J.; Nemeec, I.; Gyepes, R.; Micka, Z. <i>J. Solid State Chem.</i> 2000 , 150, 305.

		(C ₄ H ₁₂ N ₂)SeO ₄ ·H ₂ O		
82756	1.634 Å	Micka, Z.; Prokopova, L.; Cisarova, I.; Havlicek, D. <i>Coll. Czech. Chem. Commun.</i> 1996 , <i>61</i> , 1295-1306. K ₂ [Mg(H ₂ O) ₆](SeO ₄) ₂		
152720	1.634 Å	Litaïem, H.; Dammak, M.; Mhiri, T.; Cousson, A. <i>J. Alloys Compd.</i> 2005 , <i>396</i> , 34-39. (NH ₄) ₂ SeO ₄ ·Te(OH) ₆		
158479	1.634 Å	Krivovichev, S. V. <i>Ukrain. Dokl. Kristallogr.</i> 2006 , <i>135</i> , 96-101. [Al(H ₂ O) ₆](SeO ₄)(NO ₃)·H ₂ O		
250369	1.634 Å	Krivovichev, S. V. <i>Zapiski Vserossijskogo Mineralogicheskogo Obshchestva</i> 2006 , 96-101. [Al(H ₂ O) ₆] ₂ (SeO ₄)(NO ₃)·H ₂ O		
710010	1.634 Å	Euler, H.; Barbier, B.; Meents, A.; Kirfel, A. <i>Z. Kristallogr. - New Crystal Struct.</i> 2009 , <i>224</i> , 360-364. Tl ₂ [Cu(H ₂ O) ₆](SeO ₄) ₂		
710011	1.634 Å	Euler, H.; Barbier, B.; Meents, A.; Kirfel, A. <i>Z. Kristallogr. - New Crystal Struct.</i> 2009 , <i>224</i> , 360-364. Tl ₂ [Mn(H ₂ O) ₆](SeO ₄) ₂		
51079	1.635 Å	Troyanov, S. I.; Morozov, I. V.; Rybakov, V. B.; Stiewe, A.; Kemnitz, E. <i>J. Solid State Chem.</i> 1998 , <i>141</i> , 317-322. Cs ₄ (SeO ₄)(HSeO ₄) ₂ ·H ₃ PO ₄		
67234	1.635 Å	Pietraszko, A.; Lukaszewicz, K.; Augustyniak, M. A. <i>Acta Crystallogr., Sect. C</i> 1992 , <i>48</i> , 2069-2071. Li ₂ SeO ₄		
71786	1.635 Å	Baran, J.; Lis, T.; Marchewka, M.; Ratajczak, H. <i>J. Mol. Struct.</i> 1991 , <i>250</i> , 13-45. Na ₄ (SeO ₄)(SeO ₃)·H ₂ O		
82758	1.635 Å	Micka, Z.; Prokopova, L.; Cisarova, I.; Havlicek, D. <i>Coll. Czech. Chem. Commun.</i> 1996 , <i>61</i> , 1295-1306. Cs ₂ [Mg(H ₂ O) ₆](SeO ₄) ₂		
82759	1.635 Å	Micka, Z.; Prokopova, L.; Cisarova, I.; Havlicek, D. <i>Coll. Czech. Chem. Commun.</i> 1996 , <i>61</i> , 1295-1306. (NH ₄) ₂ [Mg(H ₂ O) ₆](SeO ₄) ₂		
409719	1.635 Å	Euler, H.; Meents, A.; Barbier, B.; Kirfel, A. <i>Z. Kristallogr. - New Crystal Struct.</i> 2003 , <i>218</i> , 265-268. Rb ₂ [Mg(H ₂ O) ₆](SeO ₄) ₂		
409750	1.635 Å	Euler, H.; Barbier, B.; Meents, A.; Kirfel, A. <i>Z. Kristallogr. - New Crystal Struct.</i> 2003 , <i>218</i> , 405-408. Rb ₂ [Zn(H ₂ O) ₆](SeO ₄) ₂		

411002	1.635 Å	Troyanov, S. I.; Morozov, I. V.; Rybakov, V. B.; Kemnitz, E. <i>Kristallografiya</i> 2000 , <i>45</i> , 441-447. Rb ₂ SeO ₄ ·H ₃ PO ₄
66526	1.636 Å	Zuniga, F. J.; Brezewski, T.; Amaiz, A. <i>Acta Crystallogr., Sect. C</i> 1991 , <i>47</i> , 638-640. Cs ₂ SeO ₄
409722	1.636 Å	Euler, H.; Meents, A.; Barbier, B.; Kirfel, A. Z. <i>Kristallogr. - New Cryst. Struct.</i> 2003 , <i>218</i> , 265-268. Rb ₂ [Zn(H ₂ O) ₆](SeO ₄) ₂
409747	1.636 Å	Euler, H.; Barbier, B.; Meents, A.; Kirfel, A. Z. <i>Kristallogr. - New Cryst. Struct.</i> 2003 , <i>218</i> , 405-408. Rb ₂ [Mn(H ₂ O) ₆](SeO ₄) ₂
409748	1.636 Å	Euler, H.; Barbier, B.; Meents, A.; Kirfel, A. Z. <i>Kristallogr. - New Cryst. Struct.</i> 2003 , <i>218</i> , 405-408. Rb ₂ [Co(H ₂ O) ₆](SeO ₄) ₂
171281	1.637 Å	Simmons, C. J.; Stratemeier, H.; Hitchman, M. A.; Riley, M. J. <i>Inorg. Chem.</i> 2006 , <i>45</i> , 1021-1031. K ₂ [Cu(H ₂ O) ₆](SeO ₄) ₂
171282	1.637 Å	Simmons, C. J.; Stratemeier, H.; Hitchman, M. A.; Riley, M. J. <i>Inorg. Chem.</i> 2006 , <i>45</i> , 1021-1031. K ₂ [Cu(H ₂ O) ₆](SeO ₄) ₂
246302	1.637 Å	Pertlik, F.; Fuiith, A. H. <i>Acta Crystallogr., Sect. C</i> 1989 , <i>45</i> , 158-159. Li ₂ SeO ₄
409591	1.637 Å	Fleck, M.; Kolitsch, U. Z. <i>Kristallogr. - New Cryst. Struct.</i> 2002 , <i>217</i> , 15-16. Rb ₂ [Ni(H ₂ O) ₆](SeO ₄) ₂
409591	1.637 Å	Fleck, M.; Kolitsch, U. Z. <i>Kristallogr. - New Cryst. Struct.</i> 2002 , <i>217</i> , 15-16. Rb ₂ [Cu(H ₂ O) ₆](SeO ₄) ₂
409669	1.637 Å	Euler, H.; Meents, A.; Barbier, B.; Kirfel, A. Z. <i>Kristallogr. - New Cryst. Struct.</i> 2003 , <i>218</i> , 9-10. [Mn(H ₂ O) ₄](SeO ₄) ₂ ·H ₂ O
409720	1.637 Å	Euler, H.; Meents, A.; Barbier, B.; Kirfel, A. Z. <i>Kristallogr. - New Cryst. Struct.</i> 2003 , <i>218</i> , 265-268. Rb ₂ [Co(H ₂ O) ₆](SeO ₄) ₂
409749	1.637 Å	Euler, H.; Barbier, B.; Meents, A.; Kirfel, A. Z. <i>Kristallogr. - New Cryst. Struct.</i> 2003 , <i>218</i> , 405-408. Rb ₂ [Ni(H ₂ O) ₆](SeO ₄) ₂
QIXPES	1.637 Å	Maubert, B. M.; Nelson, J.; McKee, V.; Town, R. M.; Pal, I. <i>J. Chem. Soc., Dalton Trans.</i> 2001 , 1395. (C ₃₆ H ₆₀ N ₈)SeO ₄ (ClO ₄) ₄ ·H ₂ O
89440	1.638 Å	Pietraszko, A.; Bronowska, W. <i>Solid State Commun.</i> 1999 , <i>111</i> , 205-209. Rb ₂ Li ₄ (SeO ₄) ₃ ·2H ₂ O

150084	1.638 Å	Wildner, M.; Stoilova, D.; Georgiev, M.; Karadjova, V. <i>J. Mol. Struct.</i> 2004 , <i>707</i> , 123-130. [Be(H ₂ O) ₄]SeO ₄
150706	1.638 Å	Fukami, T.; Chen Rueyhong <i>J. Phys. Soc. Jpn.</i> 2003 , <i>72</i> , 3299-3300. Na ₂ SeO ₄
171280	1.638 Å	Simmons, C. J.; Stratemeier, H.; Hitchman, M. A.; Riley, M. J. <i>Inorg. Chem.</i> 2006 , <i>45</i> , 1021-1031. K ₂ [Cu(H ₂ O) ₆](SeO ₄) ₂
409648	1.638 Å	Fleck, M.; Kolitsch, U. <i>Z. Kristallogr. - New Cryst. Struct.</i> 2002 , <i>217</i> , 471-473. (NH ₄) ₂ [Co(H ₂ O) ₆](SeO ₄) ₂
409721	1.638 Å	Euler, H.; Meents, A.; Barbier, B.; Kirfel, A. <i>Z. Kristallogr. - New Cryst. Struct.</i> 2003 , <i>218</i> , 265-268. Rb ₂ [Mn(H ₂ O) ₆](SeO ₄) ₂
409746	1.638 Å	Euler, H.; Barbier, B.; Meents, A.; Kirfel, A. <i>Z. Kristallogr. - New Cryst. Struct.</i> 2003 , <i>218</i> , 405-408. Rb ₂ [Mg(H ₂ O) ₆](SeO ₄) ₂
419776	1.638 Å	Grzechnik, A.; Brezczewski, T.; Friese, K. <i>J. Solid State Chem.</i> 2008 , <i>181</i> , 2914-2917. Tl ₂ SeO ₄
154512	1.639 Å	Dammak, M.; Mhiri, T.; Cousson, A. <i>J. Alloys Compd.</i> 2006 , <i>407</i> , 176-181. K ₂ SeO ₄ ·Te(OH) ₆
200156	1.639 Å	Mukhtarova, N. N.; Rastsvetaeva, R. K.; Ilyukhin, V. V.; Belov, N. V. <i>Dokl. Akad. Nauk SSSR</i> 1977 , <i>235</i> , 575-577. Na[In(H ₂ O) ₆](SeO ₄) ₂
201893	1.639 Å	Yamada, N.; Ono, Y.; Ikeda, T. <i>J. Phys. Soc. Jpn.</i> 1984 , <i>53</i> , 2565-2574. K ₂ SeO ₄
280788	1.639 Å	Kolitsch, U. <i>Acta Crystallogr., Sect. E</i> 2002 , <i>58</i> , 3-5. [Mg(H ₂ O) ₆]SeO ₄
409649	1.639 Å	Fleck, M.; Kolitsch, U. <i>Z. Kristallogr. - New Cryst. Struct.</i> 2002 , <i>217</i> , 471-473. (NH ₄) ₂ [Zn(H ₂ O) ₆](SeO ₄) ₂
201740	1.640 Å	Mascherpa-Corral, D.; Ducourant, M. B.; Fourcade, R.; Mascherpa, G.; Alberola, S. <i>J. Solid State Chem.</i> 1986 , <i>63</i> , 52-61. K ₂ SeO ₄ ·2SbF ₃ ·H ₂ O
60929	1.641 Å	Takahashi, I.; Onodera, A.; Shiozaki, Y. <i>Acta Crystallogr., Sect. C</i> 1987 , <i>43</i> , 179-182. Rb ₂ SeO ₄
171279	1.641 Å	Simmons, C. J.; Stratemeier, H.; Hitchman, M. A.; Riley, M. J. <i>Inorg. Chem.</i> 2006 , <i>45</i> , 1021-1031. K ₂ [Cu(H ₂ O) ₆](SeO ₄) ₂
280783	1.641 Å	Kolitsch, U. <i>Acta Crystallogr., Sect. E</i> 2001 , <i>57</i> , 104-105. [Cu(H ₂ O) ₄][SeO ₄]·H ₂ O

163455	1.642 Å	Amri, M.; Zouari, N.; Mhiri, T.; Gravereau, P. <i>J. Alloys Compd.</i> 2009 , 477, 68-75. $Cs_4(SeO_4)(HSeO_4)_2 \cdot H_3AsO_4$
201882	1.642 Å	Yamada, N.; Ikeda, T. <i>J. Phys. Soc. Jpn.</i> 1984 , 53, 2555-2564. K_2SeO_4
DEHQIR	1.642 Å	Jun-Jieh Wang; Tessier, C.; Holm, R. H. <i>Inorg. Chem.</i> 2006 , 45, 2979. $(C_8H_{20}N)_2SeO_4 \cdot CH_3CN$
838	1.644 Å	Carter, R.; Koermtgen, C.; Margulis, T. N. <i>Acta Crystallogr., Sect. B</i> 1977 , 33, 592-593. $(NH_4)_2SeO_4$
154671	1.644 Å	Dammak, M.; Litaïem, H.; Mhiri, T. <i>J. Alloys Compd.</i> 2006 , 416, 228-235. $Na_2SeO_4 \cdot Te(OH)_6 \cdot 0.5H_2O$
171283	1.644 Å	Simmons, C. J.; Stratemeier, H.; Hitchman, M. A.; Riley, M. J. <i>Inorg. Chem.</i> 2006 , 45, 1021-1031. $K_2[Cu(H_2O)_6](SeO_4)_2$
DGLYSE	1.645 Å	Olejnik, S.; Lukaszewicz, K.; Lis, T. <i>Acta Crystallogr., Sect. B</i> 1975 , 31, 1785. $(C_2H_6NO)_2SeO_4$
202659	1.646 Å	Mascherpa-Corral, D.; Ducourant, M. B.; Alberola, S. J. <i>Solid State Chem.</i> 1988 , 76, 276-283. $K_2SeO_4 \cdot 2SbF_3 \cdot 0.5H_2O$
LATUMS	1.648 Å	Kono, Y.; Takeuchi, S.; Yonehara, H.; Marumo, F.; Saito, Y. <i>Acta Crystallogr., Sect. B</i> 1971 , 27, 2341. $(C_{10}H_{12}NO)SeO_4$
15816	1.649 Å	Naray-Szabo, I.; Argay, G. <i>Acta Chim. Acad. Sci. Hung.</i> 1963 , 39, 85-92. Na_2SeO_4
99384	1.653 Å	Friese, K.; Goeta, A. E.; Leech, M. A.; Howard, J. A. K.; Madariaga, G.; Perez-Mato, J. M.; Brezewski, T. <i>J. Solid State Chem.</i> 2004 , 177, 1127-1136. Tl_2SeO_4
16042	1.654 Å	Kalman, A.; Cruickshank, D. W. J. <i>Acta Crystallogr., Sect. B</i> 1970 , 26, 436-436. Na_2SeO_4
160682	1.671 Å	Smirnov, L. S.; Melnyk, G.; Zink, N.; Wozniak, K.; Dominiak, P.; Pawlukoje, A.; Loose, A.; Shuvalov, L. A. <i>Poverkhnostnye Fizika, Khimiya, Mekhanika</i> 2007 , 73-79. $(NH_4)_2(SeO_4)_2$
Mean	1.634 Å/97	

Hydrogenselenate ion, $HSeO_4^-$

SAQHOH	1.587+1.695 Å	Baran, J.; Barnes, A. J.; Marchewka, M. K.; Pietraszko, A. J.; Ratajczak, H. J. <i>Mol. Struct.</i> 1997 , 416, 33. $(C_5H_{12}NO_2)(HSeO_4)_2(C_5H_{11}NO)_2 \cdot H_2O$
--------	---------------	--

- 163455 1.596+1.730 Å Amri, M.; Zouari, N.; Mhiri, T.; Gravereau, P. J. *Alloys Compd.* **2009**, *477*, 68-75.
Cs₄(SeO₄)(HSeO₄)₂·H₃AsO₄
- SUVQAB 1.597+1.685 Å Slouf, M.; Cisarova, I. *Acta Crystallogr., Sect. C* **1999**, *55*, 9900003. (C₁₃H₁₀N)(HSeO₄)₃·H₂O
- 31997 1.603+1.714 Å Waskowska, A.; Czaplá, Z. *Acta Crystallogr., Sect. B* **1982**, *38*, 2017-2020. RbDSeO₄
- LEJCN 1.607+1.696 Å Hamilton, E. E.; Fanwick, P. E.; Wilker, J. J. *J. Am. Chem. Soc.* **2006**, *128*, 3388.
(C₂₄H₂₀P)₃(CH₂O₈Se₂)(HSeO₄)
- NASQIH 1.608+1.688 Å Baran, J.; Drozd, M.; Lis, T.; Sledz, M.; Barnes, A. J.; Ratajczak, H. J. *Mol. Struct.* **1995**, *372*, 29.
(C₅H₁₂NO₂)(HSeO₄)₂·H₂O
- 51079 1.609+1.735 Å Troyanov, S. I.; Morozov, I. V.; Rybakov, V. B.; Stiewe, A.; Kemnitz, E. J. *Solid State Chem.* **1998**, *141*, 317-322. Cs₄(SeO₄)(HSeO₄)₂·H₃PO₄
- HESNAV 1.609+1.716 Å Fleck, M. *Acta Crystallogr., Sect. E* **2006**, *62*, o4939. CH₆N₃(HSeO₄)
- 51080 1.610+1.670 Å Troyanov, S. I.; Morozov, I. V.; Rybakov, V. B.; Stiewe, A.; Kemnitz, E. J. *Solid State Chem.* **1998**, *59150/41*, 317-322. Cs₃(HSeO₄)₂(H₂PO₄)
- XINBEB 1.610+1.725 Å Zakharov, M. A.; Troyanov, S. I.; Rybakov, V. B.; Aslanov, L. A.; Kemnitz, E. *Kristallografiya* **2001**, *46*, 1057. (C₄H₁₂N)(HSeO₄)
- XINBEB01 1.610+1.725 Å Zakharov, M. A.; Troyanov, S. I.; Rybakov, V. B.; Aslanov, L. A.; Kemnitz, E. *Kristallografiya* **2001**, *46*, 1057. (C₄H₁₂N)(HSeO₄)
- 35456 1.611+1.692 Å Brach, I.; Jones, D. J.; Roziere, J. J. *Solid State Chem.* **1983**, *48*, 401-406. RbHSeO₄
- HESNAV01 1.611+1.712 Å Drozd, M.; Baran, J.; Pietraszko, A. *Spectrochim. Acta, Part A* **2005**, *61*, 2775. CH₆N₃(HSeO₄)
- 85082 1.615+1.718 Å Hanashiro, K.; Koyano, N.; Machida, M. *Kyoto Daigaku Genshiro Jikkensho Gakujutsu Koenkai Hobunshu* **1997**, *31*, 189-192. KHSeO₄
- 88883 1.615+1.700 Å Troyanov, S. I.; Morozov, I. V.; Zakharov, M. A.; Kemnitz, E. *Kristallografiya* **1999**, *44*, 607-611.
Cs(HSeO₄)₂·H₂SeO₄
- 88882 1.616+1.719 Å Troyanov, S. I.; Morozov, I. V.; Zakharov, M. A.; Kemnitz, E. *Kristallografiya* **1999**, *44*, 607-611.
K(HSeO₄)₂·H₂SeO₄

- 88893 1.617+1.727 Å Zakharov, M. A.; Troyanov, S. I.; Rybakov, V. B.; Aslanov, L. A.; Kemnitz, E. *Kristallografiya* **1999**, 44, 448-453. NaHSeO₄
- 51081 1.617+1.635 Å Troyanov, S. I.; Morozov, I. V.; Rybakov, V. B.; Stiewe, A.; Kemnitz, E. *J. Solid State Chem.* **1998**, 141, 317-322. Cs₅(HSeO₄)₃(H₂PO₄)₂
- 65810 1.618+1.715 Å Makarova, I. P.; Rider, E. E.; Sarin, V. A.; Aleksandrova, I. P.; Simonov, V. I. *Kristallografiya* **1989**, 34, 853-861. RbHSeO₄
- 72534 1.618+1.715 Å Makarova, I. P. *Acta Crystallogr., Sect. B* **1993**, 49, 11-18. RbHSeO₄
- 72535 1.619+1.693 Å Makarova, I. P. *Acta Crystallogr., Sect. B* **1993**, 49, 11-18. NH₄HSeO₄
- 300018 1.620+1.707 Å Waskowska, A.; Olejnik, S.; Lukaszewicz, K.; Czaplá, Z. *Cryst. Struct. Commun.* **1980**, 9, 663-669. Rb(HSeO₄)
- 31998 1.621+1.715 Å Waskowska, A.; Czaplá, Z. *Acta Crystallogr., Sect. B* **1982**, 38, 2017-2020. (ND₄)DSeO₄
- 65809 1.622+1.694 Å Makarova, I. P.; Rider, E. E.; Sarin, V. A.; Aleksandrova, I. P.; Simonov, V. I. *Kristallografiya* **1989**, 34, 853-861. RbHSeO₄
- 71198 1.622+1.694 Å Makarova, I. P.; Muradyan, L. A.; Rider, E. E.; Sarin, V. A.; Alexandrova, I. P.; Simonov, V. I. *Ferroelectrics* **1990**, 107, 281-286. RbHSeO₄
- 72533 1.622+1.694 Å Makarova, I. P. *Acta Crystallogr., Sect. B* **1993**, 49, 11-18. RbHSeO₄
- 411282 1.622+1.723 Å Zakharov, M. A.; Troyanov, S. I.; Kemnitz, E. *Z. Kristallogr.* **2001**, 216, 172-175. Cs(HSeO₄)
- 72536 1.624+1.690 Å Makarova, I. P. *Acta Crystallogr., Sect. B* **1993**, 49, 11-18. NH₄HSeO₄
- 20794 1.626+1.694 Å Kruglik, A. I.; Misyul', S. V.; Aleksandrov, K. S. *Dokl. Akad. Nauk SSSR* **1980**, 255, 344-348. (NH₄)HSeO₄
- 20829 1.626+1.686 Å Aleksandrov, K. S.; Kruglik, A. I.; Misyul', S. V.; Simonov, M. A. *Kristallografiya* **1980**, 25N, 1142-1147. (NH₄)HSeO₄
- 94517 1.626+1.715 Å Troyanov, S. I.; Kosterina, E. V.; Kemnitz, E. *Zh. Neorg. Khim.* **2001**, 46, 1496-1502. Cs₄(SeO₄)(HSeO₄)₂·HF
- 2437 1.631+1.712 Å Waskowska, A.; Olejnik, S.; Lukaszewicz, K.; Glovyak, T. *Acta Crystallogr., Sect. B* **1978**, 34, 3344-

3346. RbHSeO₄59150 1.631+1.735 Å Baran, J.; Lis, T. *Acta Crystallogr., Sect. C* **1986**, *42*, 270-272. KHSeO₄**Mean 1.615+1.705 Å/33 (Mean 1.638 Å/33)****Selenic acid, H₂SeO₄**88883 1.590+1.687 Å Troyanov, S. I.; Morozov, I. V.; Zakharov, M. A.; Kemnitz, E. *Kristallografiya* **1999**, *44*, 607-611. Cs(HSeO₄)·H₂SeO₄88882 1.603+1.685 Å Troyanov, S. I.; Morozov, I. V.; Zakharov, M. A.; Kemnitz, E. *Kristallografiya* **1999**, *44*, 607-611. K(HSeO₄)·H₂SeO₄**Mean 1.597+1.686 Å/2 (Mean 1.642 Å)****Selenite ion, SeO₃²⁻**VEXCAD 1.676 Å Wiechoczek, M.; Jones, P. G. *Z. Naturforsch., Teil B* **2006**, *61*, 1401. (C₄H₁₂N)₂(SeO₃)TUYMOP 1.686 Å Havlicek, D.; Chudoba, V.; Nemeč, I.; Cisarova, I.; Micka, Z. *J. Mol. Struct.* **2002**, *606*, 101. (C₄H₁₂N₂)(SeO₃)·H₂OYASHAC 1.687 Å Todd, M. J.; Harrison, W. T. A. *Acta Crystallogr., Sect. E* **2005**, *61*, o1538. (C₃H₁₂N₂)(SeO₃)·H₂OBAYBUZ 1.689 Å Chudoba, V.; Micka, Z.; Havlicek, D.; Cisarova, I.; Nemeč, I.; Robinson, W. T. *J. Solid State Chem.* **2003**, *170*, 390. (C₄H₁₄N₂)(SeO₃)·H₂O420179 1.691 Å Burns, W. L.; Ibers, J. A. *J. Solid State Chem.* **2009**, *182*, 1457-1461. Cs(UO₂)(SeO₃)(HSeO₃)·3H₂OBAYCEK 1.692 Å Chudoba, V.; Micka, Z.; Havlicek, D.; Cisarova, I.; Nemeč, I.; Robinson, W. T. *J. Solid State Chem.* **2003**, *170*, 390. (C₃H₁₂N₂)(SeO₃)·2H₂O280981 1.698 Å Wickleder, M. S. *Acta Crystallogr., Sect. E* **2002**, *58*, 103-104. Na₂SeO₃

VEXCEH	1.698 Å	Wiechoczek, M.; Jones, P. G. Z. <i>Naturforsch., Teil B</i> 2006 , <i>61</i> , 1401. (C ₄ H ₁₂ N) ₂ (SeO ₃)·1.5H ₂ O
BAYCIO	1.700 Å	Chudoba, V.; Micka, Z.; Havlicek, D.; Cisarova, I.; Nemecek, I.; Robinson, W. T. <i>J. Solid State Chem.</i> 2003 , <i>170</i> , 390. (C ₂ H ₁₀ N ₂)(SeO ₃)

Mean 1.691 Å/9

Hydrogenselenite ion, HSeO₃⁻

ZOKZEE	1.640+1.760 Å	de Matos Gomes, E.; Matos Beja, A.; Paixao, J. A.; de Veiga, L. A.; Ramos Silva, M.; Martin-Gil, J.; Martin-Gil, F. J. <i>Z. Kristallogr.</i> 1995 , <i>210</i> , 929. (C ₁₀ H ₁₆ N)(HSeO ₃) ₂ H ₂ SeO ₃
XUJDUB	1.652+1.787 Å	Lukevics, E.; Arsenyan, P.; Shestakova, I.; Domracheva, I.; Kanep, I.; Belyakov, S.; Popelis, J.; Pudova, O. <i>Appl. Organomet. Chem.</i> 2002 , <i>16</i> , 228. (C ₆ H ₁₆ NO ₃)(HSeO ₃)
202718	1.653+1.801 Å	Micka, Z.; Danek, M.; Loub, J.; Strauch, B.; Podlahova, J.; Hasek, J. <i>J. Solid State Chem.</i> 1988 , <i>77</i> , 306-315. Cs(HSeO ₃)
ADAVAC	1.654+1.791 Å	de Matos Gomes, E.; Nogueira, E.; Fernandes, I.; Belsley, M.; Paixao, J. A.; Matos Beja, A.; Ramos Silva, M.; Martin-Gil, J.; Martin-Gil, F.; Mano, J. F. <i>Acta Crystallogr., Sect. B</i> 2001 , <i>57</i> , 828. (C ₆ H ₁₅ N ₄ O ₂)(HSeO ₃)·0.15H ₂ O
73332	1.657+1.757 Å	Loub, J.; Micka, Z.; Podlahova, J.; Maly, K.; Kopf, J. <i>Coll. Czech. Chem. Commun.</i> 1992 , <i>57</i> , 2309-2314. Na(HSeO ₄)·3H ₂ SeO ₃
RESNEI	1.657+1.768 Å	Paixao, J. A.; Matos Beja, A.; Ramos Silva, M.; de Matos Gomes, E.; Martin-Gil, J.; Martin-Gil, F. J. <i>Acta Crystallogr., Sect. C</i> 1997 , <i>53</i> , 1113. (C ₁₃ H ₁₄ N ₃)(HSeO ₃)·H ₂ O
JIVWEQ	1.658+1.784 Å	Nemecek, I.; Cisarova, I.; Micka, Z. <i>J. Solid State Chem.</i> 1998 , <i>140</i> , 71. (C ₂ H ₆ NO ₂)(HSeO ₃)·C ₂ H ₅ NO ₂
8255	1.659+1.791 Å	Chomnilpan, S.; Liminga, R. <i>Acta Crystallogr., Sect. B</i> 1979 , <i>35</i> , 3011-3013. Li(HSeO ₃)
202266	1.659+1.783 Å	Hiltunen, L.; Holsa, J.; Micka, Z. <i>J. Solid State Chem.</i> 1987 , <i>68</i> , 307-313. Cs(HSeO ₄)·2H ₂ SeO ₃
DEHQOX	1.659+1.758 Å	Jun-Jieh Wang; Tessier, C. T.; Holm, R. H. <i>Inorg. Chem.</i> 2006 , <i>45</i> , 2979. (C ₈ H ₂₀ N)(HSeO ₃)

XORBUB	1.659+1.769 Å	Nemec, I. Chudoba, V.; Havlicek, D.; Cisarova, I.; Micka, Z. <i>J. Solid State Chem.</i> 2001 , <i>161</i> , 312. (C ₆ H ₁₆ N ₂)(HSeO ₃) ₂
403078	1.660+1.782 Å	Kek, S. Z. <i>Kristallogr.</i> 1997 , <i>212</i> , 724-731. Li(HSeO ₃)
EKIBAB	1.667+1.763 Å	Ritchie, L. K.; Harrison, W. T. A. <i>Acta Crystallogr., Sect. E</i> 2001 , <i>59</i> , o1296. (C ₂ H ₇ N ₄ O)(HSeO ₃)
KELKAO	1.668+1.765 Å	Paixao, J. A.; Silva, M. R.; Beja, A. M.; Eusebio, E. <i>Polyhedron</i> 2006 , <i>25</i> , 2021. (C ₁₁ H ₁₃ N ₂ O ₂)(HSeO ₃)
250286	1.670+1.749 Å	Krivovichev, S. V.; Tananaev, I. G.; Kahlenberg, V.; Myasoedov, B. F. <i>Dokl. Akad. Nauk</i> 2005 , <i>403</i> , 349-352. ((C ₃ H ₁₁)NH ₃)(UO ₂)(SeO ₄)(HSeO ₃)
62335	1.671+1.781 Å	Bannova, I. I.; Vinogradova, I. S.; Kuzmin, A. M.; Rozhdestvenskaya, I. V.; Usov, O. A. <i>Kristallografiya</i> 1987 , <i>32N</i> , 83-85. Rb(HSeO ₃)
171372	1.672+1.761 Å	Weil, M. <i>Acta Crystallogr., Sect. E</i> 2006 , <i>62</i> , 138-140. NH ₄ (HSeO ₃)
62289	1.676+1.750 Å	Rider, E. E.; Sarin, V. A.; Bydanov, N. N.; Vinogradova, I. S. <i>Kristallografiya</i> 1986 , <i>31N</i> , 264-269. Na(DSeO ₃)
62288	1.679+1.746 Å	Rider, E. E.; Sarin, V. A.; Bydanov, N. N.; Vinogradova, I. S. <i>Kristallografiya</i> 1986 , <i>31N</i> , 264-269. Na(HSeO ₃)
420179	1.679+1.767 Å	Burns, W. L.; Ibers, J. A. <i>J. Solid State Chem.</i> 2009 , <i>182</i> , 1457-1461. Cs(UO ₂)(SeO ₃)(HSeO ₃)·3H ₂ O
KELKAO01	1.679+1.763 Å	Paixao, J. A.; Silva, M. R.; Beja, A. M.; Eusebio, E. <i>Polyhedron</i> 2006 , <i>25</i> , 2021. (C ₁₁ H ₁₃ N ₂ O ₂)(HSeO ₃)
Mean	1.663+1.770 Å/21	(Mean 1.699 Å)
Selenous acid, H₂SeO₃		
ZOKZEE	1.612+1.739 Å	de Matos Gomes, E.; Matos Beja, A.; Paixao, J. A.; de Veiga, L. A.; Ramos Silva, M.; Martin-Gil, J.; Martin-Gil, F. J. <i>Kristallogr.</i> 1995 , <i>210</i> , 929. (C ₁₀ H ₁₆ N)(HSeO ₃)·H ₂ SeO ₃
73332	1.618+1.735 Å	Loub, J.; Micka, Z.; Podlahova, J.; Maly, K.; Kopf, J. <i>Coll. Czech. Chem. Commun.</i> 1992 , <i>57</i> , 2309-2314. Na(HSeO ₄)·3H ₂ SeO ₃

NIRSIQ	1.622+1.735 Å	Paixao, J. A.; Matos Beja, A.; Ramos Silva, M.; Alte da Veiga, L.; Martin-Gil, J.; Martin-Gil, F.; de Matos Gomes, E. <i>Z. Kristallogr. - New Cryst. Struct.</i> 1997 , <i>212</i> , 51. $C_3H_{11}NO_2 \cdot H_2SeO_3$
202266	1.632+1.748 Å	Hiltunen, L.; Holsa, J.; Micka, Z. <i>J. Solid State Chem.</i> 1987 , <i>68</i> , 307-313. $Cs(HSeO_4) \cdot 2H_2SeO_3$
71786	1.666+1.740 Å	Baran, J.; Lis, T.; Marchewka, M.; Ratajczak, H. <i>J. Mol. Struct.</i> 1991 , <i>250</i> , 13-45. $Na_2SeO_4 \cdot H_2SeO_3$
Mean	1.621+1.739 Å/4	(Mean 1.700 Å)

